Article

Neuron

Positive Allosteric Modulators of GluN2A-Containing NMDARs with Distinct Modes of Action and Impacts on Circuit Function

Highlights

- Describe discovery of novel GluN2A-selective NMDAR positive allosteric modulators (PAMs)
- Crystal structures identify a new modulatory site in the GluN2A GluN1 LBD interface
- Distinct PAMs have unique effects on NMDAR biophysical properties
- Distinct PAMs have unique impacts on LTP

Authors

David H. Hackos, Patrick J. Lupardus, Teddy Grand, ..., Morgan Sheng, Qiang Zhou, Jesse E. Hanson

Correspondence

hanson.jesse@gene.com

In Brief

Hackos et al. describe the discovery of positive allosteric modulators of GluN2A NMDA receptors that bind a novel site in the GluN1/GluN2A ligand-binding domain. Modulators with distinct pharmacological properties are then used to probe NMDAR function in brain slices.

Accession Numbers

5H8F
5H8H
5H8N
5H8Q
5H8R
5H8S

Hackos et al., 2016, Neuron *89*, 983–999
March 2, 2016
http://dx.doi.org/10.1016/j.neuron.2016.01.016

CellPress

Neuron
Article

Positive Allosteric Modulators of GluN2A-Containing NMDARs with Distinct Modes of Action and Impacts on Circuit Function

David H. Hackos,[1,6] Patrick J. Lupardus,[2,6] Teddy Grand,[5] Yelin Chen,[1,7] Tzu-Ming Wang,[1] Paul Reynen,[3] Amy Gustafson,[3] Heidi J.A. Wallweber,[2] Matthew Volgraf,[4] Benjamin D. Sellers,[4] Jacob B. Schwarz,[4] Pierre Paoletti,[5] Morgan Sheng,[1] Qiang Zhou,[1,8] and Jesse E. Hanson[1,*]
[1]Department of Neuroscience
[2]Department of Structural Biology
[3]Department of Biochemical and Cellular Pharmacology
[4]Department of Discovery Chemistry
Genentech, Inc., 1 DNA Way, South San Francisco, CA 94080, USA
[5]Ecole Normale Supérieure, PSL Research University, Institut de Biologie de l'Ecole Normale Supérieure (IBENS), Centre National de la Recherche Scientifique (CNRS) UMR8197, INSERM U1024, 75005 Paris, France
[6]Co-first author
[7]Present address: Interdisciplinary Research Center on Biology and Chemistry, Shanghai Institute of Organic Chemistry, Chinese Academy of Sciences, Shanghai 200032, China
[8]Present address: School of Chemical Biology and Biotechnology, Peking University Shenzhen Graduate School, Shenzhen, China
*Correspondence: hanson.jesse@gene.com
http://dx.doi.org/10.1016/j.neuron.2016.01.016

SUMMARY

To enhance physiological function of NMDA receptors (NMDARs), we identified positive allosteric modulators (PAMs) of NMDARs with selectivity for GluN2A subunit-containing receptors. X-ray crystallography revealed a binding site at the GluN1-GluN2A dimer interface of the extracellular ligand-binding domains (LBDs). Despite the similarity between the LBDs of NMDARs and AMPA receptors (AMPARs), GluN2A PAMs with good selectivity against AMPARs were identified. Potentiation was observed with recombinant triheteromeric GluN1/GluN2A/GluN2B NMDARs and with synaptically activated NMDARs in brain slices from wild-type (WT), but not GluN2A knockout (KO), mice. Individual GluN2A PAMs exhibited variable degrees of glutamate (Glu) dependence, impact on NMDAR Glu EC_{50}, and slowing of channel deactivation. These distinct PAMs also exhibited differential impacts during synaptic plasticity induction. The identification of a new NMDAR modulatory site and characterization of GluN2A-selective PAMs provide powerful molecular tools to dissect NMDAR function and demonstrate the feasibility of a therapeutically desirable type of NMDAR enhancement.

INTRODUCTION

NMDA receptors (NMDARs) are glutamate-gated ion channels that play critical roles in synaptic signaling and plasticity and NMDAR dysfunction is implicated in a variety of nervous system disorders (Paoletti et al., 2013; Soto et al., 2014; Traynelis et al., 2010; Zhou and Sheng, 2013). NMDAR hypofunction in particular may play a role in the pathophysiology of schizophrenia (Coyle et al., 2003; Gonzalez-Burgos and Lewis, 2012). This idea originally arose from observations that NMDAR antagonists can transiently induce the positive, negative, and cognitive symptoms of schizophrenia in healthy individuals (Javitt and Zukin, 1991; Krystal et al., 1994), and it subsequently has been supported by behavioral alterations in animal models with genetically or pharmacologically reduced NMDAR function (Belforte et al., 2010; Mohn et al., 1999; Rujescu et al., 2006). NMDAR hypofunction also has been implicated in other neurological disorders. For example, NMDAR mutations, including microdeletions and predicted loss-of-function mutations, have been identified in patients with epilepsy-aphasia disorders (Carvill et al., 2013; Lemke et al., 2013; Lesca et al., 2013), and impairment of synaptic NMDAR function has been found in animal models of Alzheimer's disease (Zádori et al., 2014). Decreased NMDAR function may in principle be corrected by pharmacologically boosting activation of the remaining functional NMDARs, yet this approach risks eliciting excitotoxicity through excessive activation of NMDARs (Heng et al., 2009; Liu et al., 2007; Milnerwood et al., 2010; Tu et al., 2010; Zeron et al., 2002). Therefore, to selectively enhance physiological NMDAR function, we set out to discover molecules that act as positive allosteric modulators (PAMs) to enhance the natural physiological pattern of activation of these receptors while avoiding indiscriminate activation caused by stimulation with orthosteric agonists.

To further ensure enhancement of physiological, but not pathological, activation of NMDARs, we sought to discover PAMs with selectivity for GluN2A subunit-containing NMDARs. The GluN2 subunit composition is a critical determinant of the physiological and pathological contributions of NMDAR activation

(Paoletti et al., 2013). During brain development, there is a switch from an early dominance of GluN2B subunit expression to incorporation of GluN2A subunits at mature synapses (Sheng et al., 1994; Williams et al., 1993). It recently has become clear that mature synapses contain not only GluN2A diheteromers (GluN1/GluN2A composition), but also a significant portion of triheteromers (GluN1/GluN2A/GluN2B), which play key roles in synaptic plasticity and signaling (Gray et al., 2011; Rauner and Köhr, 2011; Soares and Lee, 2013; Tovar et al., 2013). At the same time, experiments using antagonists that preferentially inhibit GluN2B diheteromers (GluN1/GluN2B) (Hansen et al., 2014; Hatton and Paoletti, 2005; Stroebel et al., 2014) have shown that this type of NMDAR can mediate excitotoxicity when excessively activated (Costa et al., 2012; Ferreira et al., 2012; Rönicke et al., 2011). Hypotheses for the deleterious effects of activating GluN2B diheteromers include the nature of the downstream signaling pathways to which they couple and/or their preferential extrasynaptic localization (Hardingham and Bading, 2010; Martel et al., 2012; Zhou and Sheng, 2013). In any case, pharmacological over-activation of GluN2B diheteromers in particular could risk pathogenic consequences. Therefore, the discovery of NMDAR enhancers that selectively potentiate GluN2A-containing NMDARs without affecting GluN2B diheteromeric receptors would not only provide a valuable tool for dissecting physiological NMDAR function, but also could represent an attractive therapeutic approach.

Here we describe a novel class of compounds that act as PAMs at GluN2A-containing NMDARs and thus enhance the normal synaptic activation of NMDARs without causing activation in the absence of stimulation. X-ray crystallography reveals that these compounds act via a novel NMDAR positive modulator binding site at the interface between the GluN1 and GluN2A ligand-binding domains (LBDs), a site that is analogous to a known PAM site found in AMPA receptors (AMPARs). These GluN2A PAMs potentiate recombinant diheteromeric and triheteromeric NMDARs as well as native NMDARs in brain slices during synaptic activation. Distinct but chemically related GluN2A PAMs alter channel deactivation kinetics and Glu affinity to varying degrees and also show differing dependence on Glu concentration. These distinct GluN2A PAMs also show differential impacts on synaptic plasticity that correlate with differences in their ability to affect synapses on pyramidal neurons versus interneurons. GluN2A PAMs therefore represent novel tools that can provide insight into the mechanisms of NMDAR activation and the subunit-specific roles of NMDARs in circuit function. This new class of selective NMDAR modulator also demonstrates that NMDARs can be pharmacologically targeted in a manner that may be therapeutically desirable for neurological disorders involving NMDAR hypofunction.

RESULTS

Discovery of Potent and Selective GluN2A PAMs

To screen for compounds that can enhance NMDAR activation in response to application of Glu in the presence of saturating glycine (Gly), we established a cell-based Ca^{2+} influx assay using HEK293 cells stably expressing GluN1 and GluN2A. A library of 1.4 million compounds was tested for the ability to increase the Ca^{2+} influx fluorescence signal significantly above the signal obtained by subsaturating (EC30) Glu alone. GNE-3476 was identified as a hit in this high-throughput screen (HTS), with 6 μM compound leading to a marked enhancement of the response to EC30 Glu (Figures 1A and 1B). Follow-up assays showed a dose-dependent enhancement of NMDAR activation by GNE-3476 (estimated EC_{50} = 10.3 μM) (Figure 1C). Subsequent medicinal chemistry efforts (Supplemental Experimental Procedures) led to GluN2A PAMs with enhanced potency in the Ca^{2+} influx assay compared to GNE-3476, as exemplified by GNE-3419 (2.03 μM EC_{50}), GNE-6901 (0.33 μM), and GNE-8324 (2.43 μM) (Figure 1C). Electrophysiological measurements of NMDAR currents in *Xenopus* oocytes expressing GluN1 and GluN2A confirmed that these compounds act as allosteric modulators rather than orthosteric agonists, with robust potentiation of the response to saturating Glu (100 μM) under various conditions where compound alone resulted in little to no signal (Figures 1D and S1). We next assessed selectivity of these more potent GluN2A PAMs by determining the dose-response relationship from cell lines expressing GluN1 paired with GluN2B, GluN2C, or GluN2D (Figures 1E–1G). Little or no compound-induced potentiation was detected in the GluN2B and GluN2C cell lines. While significant potentiation of GluN1/GluN2D NMDARs was seen with GNE-3419 and GNE-6901, the potency was 10-fold lower with GluN2D compared to GluN2A NMDARs.

GluN2A PAMs Bind at the Inter-domain Interface of the GluN1/GluN2A LBDs

The amino-terminal domains (ATDs) of NMDARs can bind an array of ligands that act as subunit-specific allosteric modulators (Zhu and Paoletti, 2015). Yet functional characterization of NMDARs with chimeric ATDs or ATD deletions demonstrated that the ATD was not required for PAM effects (Figures S2A and S2B). To examine the LBD as a potential binding site, we crystallized and solved a 2.1-Å structure of the isolated human GluN1/GluN2A LBD dimer in complex with GNE-6901. The binding site of GNE-6901 was found to lie at the inter-domain interface between GluN1 and GluN2A LBDs (Figures 2A and 2B). This site is analogous to the binding site of AMPAR PAM molecules such as cyclothiazide (Sun et al., 2002) and aniracetam (Jin et al., 2005). Yet while the AMPAR PAMs bind a symmetric interface formed between two GluA1 LBD homodimers, the heterodimeric GluN1/GluN2A LBD interface exhibits elements of both symmetry and asymmetry (Figures 2C–2E). Comparison of the binding site of GNE-6901 to an apo GluN1/GluN2A structure (Figure 2C) reveals that the side chains of GluN1 Y535 and GluN2A E530 change rotamer conformations to permit binding of GNE-6901. To test whether these rotamer movements are important for PAM effects on the channel, we mutated GluN1 Y535 and GluN2A E530 to alanine individually or in combination, and we performed functional analysis using oocyte electrophysiology. These alanine mutants showed increased potentiation of NMDAR currents by GNE-6901 while minimally affecting the compound EC_{50} (Figure S2G), suggesting that rearrangements of the GluN1 Y535 and GluN2A E530 side chains (which are required for formation of the GNE-6901 binding site) do not appear to be required for mediating potentiation.

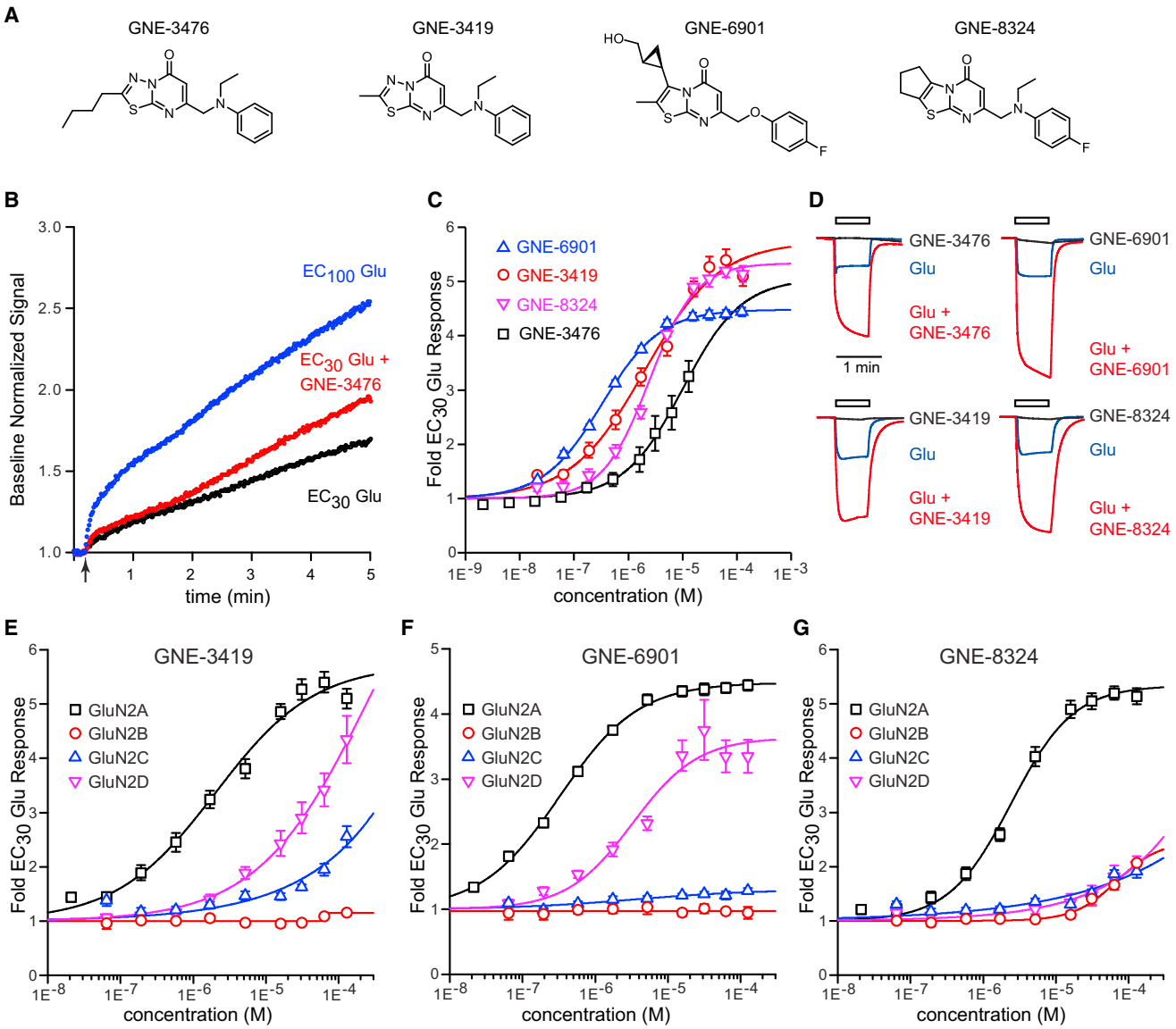

Figure 1. Discovery of Potent and GluN2A-Selective NMDAR PAMs

(A) Chemical structures of the GluN2A PAMs characterized in this study are shown.

(B) Ca^{2+} influx measurements from GluN1/GluN2A-expressing HEK cells show an enhanced response to EC_{30} Glu stimulation (arrow indicates onset) when 6 μM GNE-3476 was co-applied during the HTS.

(C) Fold potentiation of the EC_{30} Glu response is shown as a function of dose for GNE-3476, GNE-3419, GNE-8324, and GNE-6901. Data are shown as mean ± SEM (n = 12 dose-response curves/compound).

(D) NMDAR currents were measured in oocytes expressing GluN1 and GluN2A to confirm that compounds acted as PAMs rather than agonists. Under conditions where little or no current was induced by 30 μM compound in the absence of exogenous Glu application, co-application of 100 μM Glu with 30 μM compound resulted in significant potentiation relative to Glu alone. 50 μM Gly was present continuously and 5 μM AP5 was present to minimize activation by ambient Glu. Scale bar represents 1 min and current values on the y axes have been normalized to Glu-alone response amplitudes for each experiment.

(E–G) Ca^{2+} influx dose-response data for GNE-3419 (E), GNE-6901 (F), and GNE-8324 (G) are shown for HEK cell lines expressing GluN1 paired with GluN2A (reproduced from B), GluN2B, GluN2C, or GluN2D.

Data are shown as mean ± SEM (n = 4–12 dose-response curves/compound/GluN2 subtype).

While no previous NMDAR modulators have been shown to bind at the GluN1/GluN2A LBD interface, chimera and mutational analyses have identified interface residues required for the action of the GluN2A-selective negative allosteric modulator (NAM) TCN-201 (Hansen et al., 2012). To compare the binding modes of this well-characterized class of NAM with GNE-6901, we attempted co-crystallization of the GluN1/GluN2A LBD with TCN-201 and related compounds. While TCN-201 (compound 1; Bettini et al., 2010) did not lead to an X-ray structure, we were able to obtain a 2.5-Å structure of the highly related GluN2A

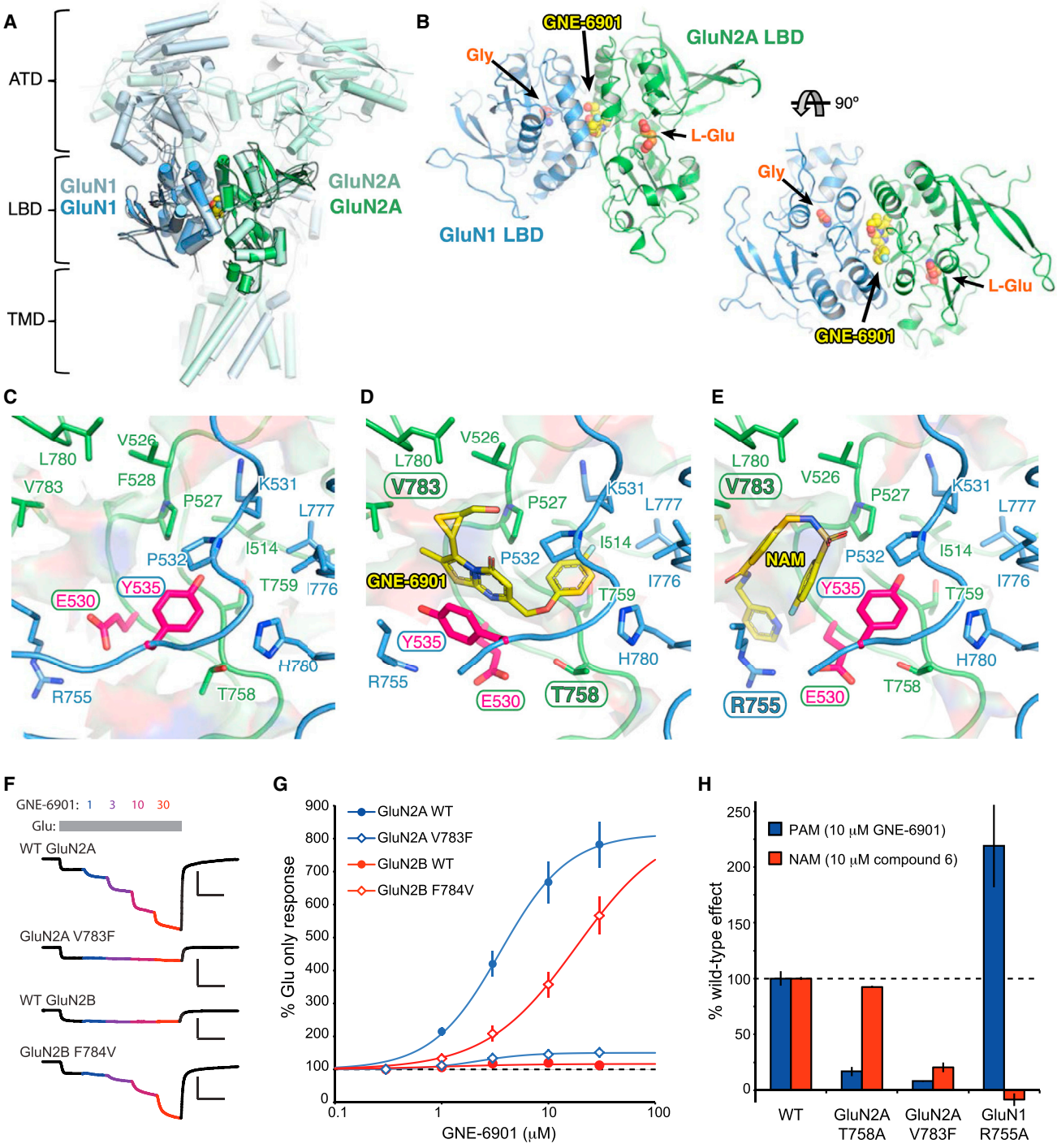

Figure 2. Identification of an NMDAR Modulator-Binding Site at the GluN1/GluN2A LBD Interface

(A) Cartoon representation of the human GluN1/GluN2A ligand-binding domain (LBD) structure bound to GNE-6901 presented in this paper overlaid with the full-length *Xenopus* GluN1/GluN2B receptor (PDB: 4TLL, Lee et al., 2014). The amino-terminal domains (ATDs) and trans-membrane domains (TMDs) also are labeled to show the overall position of the LBD in the context of the full-length channel. For the human LBD bound to GNE-6901, GluN1 is shown in dark blue, GluN2A is shown in dark green, and compound is shown as yellow spheres; for the full-length receptor, GluN1 is colored light blue and GluN2B light green. Colors used are consistent throughout this figure.

(B) The LBD crystal structure in complex with GNE-6901 is shown in the same orientation as depicted in (A) (upper left) and rotated 90° to show a top view (bottom right). Glutamate (L-Glu), Glycine (Gly), and GNE-6901 are shown as spheres and binding sites are labeled.

(legend continued on next page)

NAM, compound 6 (Bettini et al., 2010). This structure revealed that compound 6 binds to a distinct but overlapping region of the inter-domain interface as the GluN2A PAMs (Figure 2E). Interestingly, the side chain rotamer conformation of GluN1 Y535 is similar to that found in the apo conformation, while GluN2A E530 moves into a conformation similar to that of the PAM-bound structure to accommodate the pyridine ring of compound 6. Together, these structures identify similar but unique binding sites for GluN2A-selective PAMs and NAMs.

In comparing our compound-bound GluN1/GluN2A LBD structure with the full-length GluN1/GluN2B structure (Karakas and Furukawa, 2014; Lee et al., 2014), we identified an important difference in the PAM-binding site targeted by GNE-6901. V783 in GluN2A is a key border residue of the PAM-binding site, and it is in direct van der Waals contact with the methyl group on the thiazolopyrimidinone core of GNE-6901 (Figure 2D). The much larger corresponding residue, F784 in GluN2B, protrudes into the binding site and may prevent PAM binding to GluN1/GluN2B NMDARs. To test the functional importance of this residue in PAM selectivity, we expressed GluN2A NMDARs with a V783F mutation, as well as GluN2B NMDARs with the converse F784V mutation, in oocytes and tested their sensitivity to GNE-6901. The V783F mutation in GluN2A virtually abolished GNE-6901 sensitivity, while the F784V mutation in GluN2B conferred an ability of GNE-6901 to potentiate GluN1/GluN2B NMDARs (Figures 2F and 2G). This striking swap of sensitivity between GluN2A and GluN2B NMDARs by exchange of a single residue demonstrates that GluN2A V783 is a key determinant of PAM selectivity. Further experiments show that the corresponding residue in GluN2D, which corresponds to a Leucine (L811), is also a determinant of the less potent PAM effect of GNE-6901 observed on GluN2D receptors (Figures S2C–S2F).

Interestingly, GluN2A V783 was identified previously as essential for the action of the NAM TCN-201 (Hansen et al., 2012). To better characterize the overlapping binding sites of our series of PAMs and the prior series of NAMs, we performed mutational analysis to confirm unique and shared structural determinants. Consistent with predictions from our structures and prior work with TCN-201, we found that while GluN2A V783F blocks the effects of both GNE-6901 and the NAM (compound 6), GluN2A T758A blocks the PAM effect, but not the NAM effect, and GluN1 R755A blocks the NAM effect, but not the PAM effect (Figures 2H and S2H–S2J). This demonstration of both common and specific structural determinants of PAMs and NAMs confirms the overlapping nature of the binding sites.

Selectivity against AMPARs

Given that the GluN1/GluN2 heterodimer interface where GNE-6901 binds is equivalent to the binding site of AMPAR PAMs, we tested the selectivity of our GluN2A PAMs against AMPARs using a Ca^{2+} influx assay in cell lines expressing GluA2 AMPARs. These experiments revealed that, while GNE-3419 potentiates both flip and flop variants of GluA2, GNE-6901 and GNE-8324 show no appreciable activity on these AMPARs (Figures 3A and 3B). To further dissect mechanisms of NMDAR versus AMPAR selectivity, we attempted to co-crystallize these compounds with the AMPAR LBD dimer (Armstrong and Gouaux, 2000). Consistent with the functional effect on AMPARs, soaking of GNE-3419 in AMPAR crystals resulted in a compound-bound structure, which revealed that GNE-3419 binds in the AMPAR dimer interface (Figure 3C) in a position equivalent to the PAM-binding site in GluN1/GluN2A (Figure 3D). The corresponding residue to GluN2A V783 in the AMPAR flip isoform is Serine 786, and our structure demonstrates that this Ser residue is not large enough to disrupt the AMPAR-binding pocket. While we did not crystallize the AMPAR LBD with the flop Asn residue at this position (Asn786), our functional assays indicate Asn also does not disrupt GNE-3419 potentiation (Figure 3B). To test for potentiation of native AMPARs during physiological activation, we examined AMPAR excitatory postsynaptic potentials (EPSPs) in hippocampal CA1 pyramidal neurons during Schaffer collateral stimulation. These experiments were consistent with the cell-based assay, with robust potentiation of AMPAR EPSPs by GNE-3419 and no detectable impact of GNE-6901 (Figures 3E and 3F).

Surprisingly, the potentiation of the AMPAR EPSP by GNE-3419 could be reversed with the addition of GNE-6901. Conversely, pre-incubation with GNE-6901 prevented potentiation by subsequent addition of GNE-3419 (Figures S3A–S3D). This dose-dependent antagonism of the GNE-3419 potentiation of AMPARs by GNE-6901, coupled with the absence of any impact of GNE-6901 alone on the AMPAR EPSPs, indicates that GNE-6901 may act as a silent allosteric modulator (SAM) of AMPARs. In other words, the functional selectivity achieved for GluN2A PAMs against AMPARs may be due to a lack of efficacy rather than potency at AMPARs.

Given the high degree of sequence similarity between AMPA and kainate receptors (KARs) at the PAM-binding site (Figure S2C), we tested if GNE-3419 might potentiate KARs as well as AMPARs using voltage-clamp measurements from oocytes expressing GluK2. While the positive control PAM,

(C) View of the PAM-binding site from an unbound apo structure of the human GluN1/GluN2A LBD. Key interface residues are shown as stick models and residues that move upon PAM binding (GluN1 Y535 and GluN2A E530) are highlighted in magenta. Solvent-accessible surface area in the interface is shown as a transparent surface. (C)–(E) are rotated 90° to the right compared to the LBD representation in (A).

(D) View of GNE-6901 bound in the PAM-binding site of the GluN1/GluN2A LBD is shown.

(E) The GluN2A-selective NAM (compound 6, Bettini et al., 2010) bound to GluN1/GluN2A LBD is shown. Note that the NAM binds in a partially overlapping region of the heterodimer interface as the PAM.

(F) Example traces from NMDAR currents measured in oocytes expressing mutant or WT GluN2A or GluN2B are shown; 1, 3, 10, and 30 μM GNE-6901 were sequentially added during application of 300 nM Glu. Scale bars represent 1 min and 1 μA (top two traces) or 0.5 μA (bottom two traces).

(G) Dose-response data for each type of channel are shown. Data are shown as mean ± SEM (n = 10–12 oocytes/dose-response curve).

(H) Impacts of point mutations of the residues highlighted in (D) and (E) on PAM and NAM effects. PAM effects are normalized to the average potentiation observed with 10 μM GNE-6901 and NAM effects to the average inhibition observed with 10 μM compound 6. Data are summarized from (G) and Figures S2H and S2I and are shown as mean ± SEM.

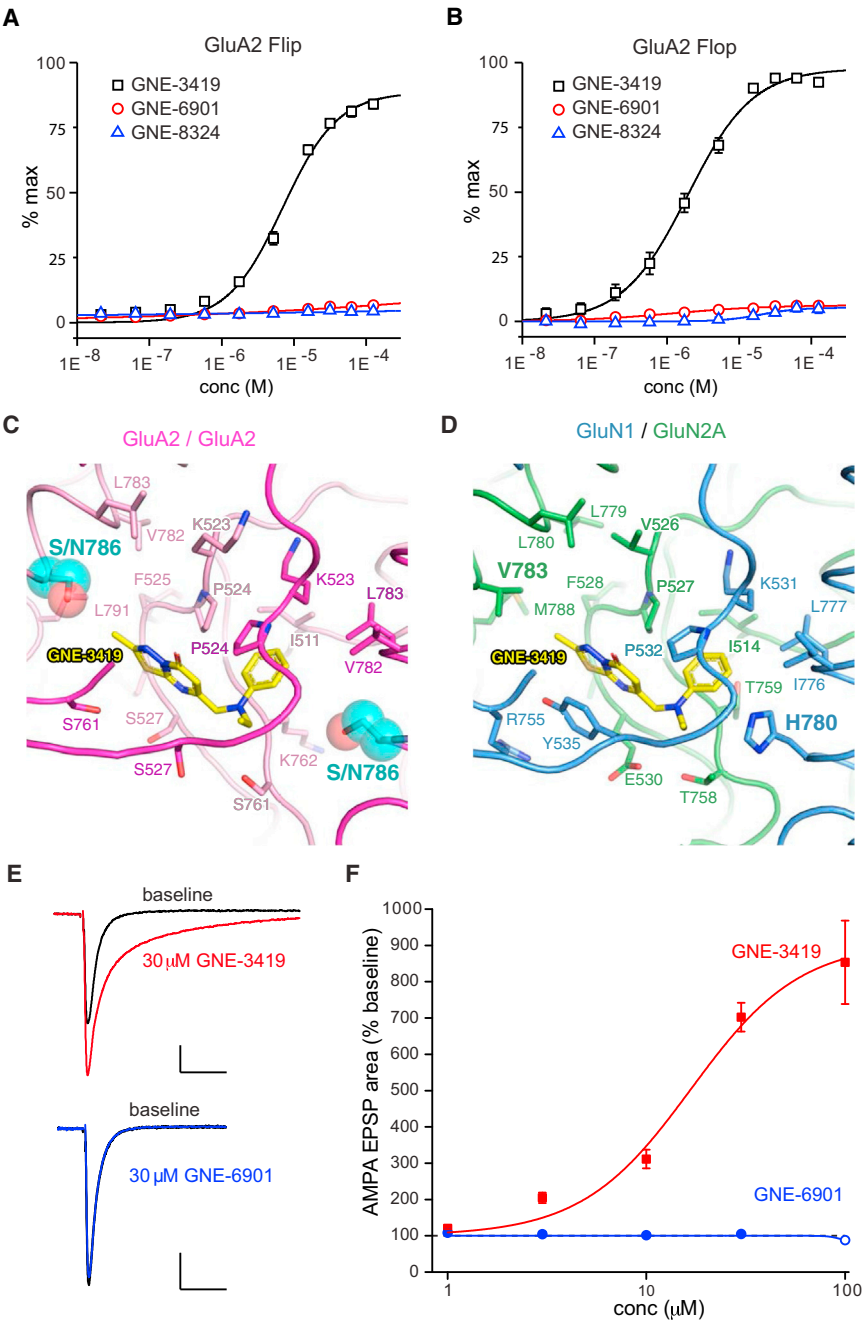

Figure 3. Characterization of Selectivity against AMPARs

(A and B) Ca^{2+} influx measurements from cell lines expressing the flip (A) or flop (B) variant of GluA2 are shown in response to Glu application in the presence of increasing PAM concentrations. Data are shown as mean ± SEM (n = 4–10 dose-responses/compound).

(C) The crystal structure of GNE-3419 in complex with the GluA2 LBD is shown. The individual GluA2 monomers are shown as cartoon models in light pink and dark pink. Residues that interact with GNE-3419 are shown as stick models. The binding site includes a residue that differs between flip (S786, corresponding to this structure) and flop (N786) isoforms (highlighted in cyan).

(D) The structure of GNE-3419 in complex with the GluN1/GluN2A LBD is shown in the same orientation as the GluA2 structure in (C). Residues that interact with GNE-3419 are shown as stick models. The GluN1/GluN2A residues analogous to the flip residue S786 are highlighted with large labels.

(E) Evoked AMPA EPSPs recorded from CA1 pyramidal neurons in hippocampal brain slices are shown. Average EPSPs before (black) and after application of 30 μM GNE-3419 (red) or GNE-6901 (blue) are shown. Scale bars represent 50 ms and 0.5 mV.

(F) Dose-response data show the percentage potentiation of AMPAR EPSP area in response to GNE-3419 (red) or GNE-6901 (blue) application. Open circle indicates that incomplete solubility was observed for GNE-6901 at the highest concentration tested. Data are shown as mean ± SEM (n = 5–9 brain slices/dose/compound).

Concanavalin A (ConA), which blocks KAR desensitization, revealed robust Glu-evoked currents, GNE-6901, GNE-8324, and GNE-3419 all failed to act on GluK2 in a similar manner. Parallel experiments with GluA2 confirmed that GNE-3419, but not the other PAMs, could block AMPAR desensitization in this same experimental paradigm (Figures S3E and S3F), supporting selectivity against KARs.

Potentiation of Triheteromeric and Synaptic NMDARs

While the cell-based assays used to test GluN2A PAMs demonstrated potentiation of GluN2A, but not GluN2B-containing NMDARs, the cell lines used in these assays express pure populations of diheteromeric receptors. Synaptic NMDARs, however, are thought to contain a significant proportion of triheteromeric NMDARs comprised of both GluN2A and GluN2B subunits (Gray et al., 2011; Rauner and Köhr, 2011; Soares and Lee, 2013; Tovar et al., 2013). Therefore, we compared the effects of GNE-6901 on GluN2A diheteromers, GluN2A/GluN2B triheteromers, and GluN2B diheteromers, using a system for controlling NMDAR subunit composition with ectopic retention signals (Stroebel et al., 2014). These experiments revealed that triheteromeric receptors also are potentiated by GNE-6901 (Figures 4A and 4B). Consistent with the presence of a single PAM-binding site in each triheteromer as compared to the two binding sites per GluN2A diheteromer, potentiation of triheteromers was of a smaller magnitude than that of GluN2A diheteromers. Similarly, we also observed that GNE-8324 could potentiate both diheteromers and triheteromers (Figures S4A and S4B). In addition, potentiation by both PAMs was independent of the GluN1 splice variant (Figures S4C–S4F).

To directly test the impact of GNE-6901 on synaptically activated NMDARs, we performed whole-cell recordings of pharmacologically isolated NMDAR excitatory postsynaptic currents (EPSCs) in CA1 pyramidal neurons in response to Schaffer collateral stimulation in brain slices. To test specificity for GluN2A NMDARs, recordings were performed in slices from GluN2A knockout (KO) mice as well as wild-type (WT) mice. In WT mice, a clear potentiation of the NMDAR EPSC was observed when GNE-6901 was applied to brain slices, with a greater relative potentiation of EPSC area compared to peak amplitude that was associated with a slowing of the decay time of the EPSC (Figures 4C–4G). In GluN2A KO mice there was a longer baseline decay time constant for the NMDAR EPSCs compared to WT mice (254.8 ± 45.6 versus 74.6 ± 8.5 ms), which is consistent with the presence of synaptic GluN2B diheteromers in the absence of GluN2A subunits in these mice. There was no effect of GNE-6901 application on NMDAR EPSCs in the GluN2A KO mice, with only a small rundown of the NMDAR EPSC evident during the recording period (Figures 4C–4H).

Different GluN2A PAMs Have Distinct Impacts on NMDAR Channel Function

To examine modulation of NMDAR channel function with higher resolution, we performed whole-cell patch-clamp recordings on CHO cells stably expressing GluN1 and GluN2A using a rapid solution switching system. These experiments confirmed the PAM effects on NMDARs. While Glu or Gly alone applied in the presence of GNE-6901 or GNE-8324 resulted in minimal current, the magnitude of the current elicited by Glu and Gly co-application was enhanced in the presence of the GluN2A PAMs (Figure S5). Dose-response experiments using a brief pulse (2 s) of 100 μM Glu in the presence of 50 μM Gly confirmed the greater potency of GNE-6901 compared to GNE-8324 (Figures 5A–5C). Notably, both PAMs can increase NMDAR currents even during the presence of saturating agonist concentrations. However, striking differences between GNE-6901 and GNE-8324 were apparent during channel deactivation following the removal of Glu in the constant presence of Gly. While GNE-6901 resulted in a relatively modest slowing of the rate of deactivation following the removal of Glu, GNE-8324 caused a profound slowing of glutamate deactivation kinetics (Figures 5A, 5B, and 5D). In contrast, when Gly was removed in the constant presence of Glu, NMDAR currents rapidly deactivated in the presence of either PAM (Figures 5E and 5F), demonstrating a specific interaction of PAMs with Glu, but not Gly.

To further examine the interactions of GNE-6901 and GNE-8324 with the agonists, Gly and Glu potencies were assessed in the presence or absence of near saturating concentrations of each PAM (10 μM GNE-6901 and 30 μM GNE-8324). These experiments showed that neither PAM had significant impacts on Gly potency (Figures 6A–6C, S6A, and S6D). On the other hand, GNE-8324 significantly increased the potency of Glu at the NMDAR, while GNE-6901 had a much smaller impact on Glu potency (Figures 6D–6F, S6B, and S6E). We next examined the converse question of whether GNE-8324 potency was more dependent on Glu concentration than GNE-6901. In these experiments, we observed potentiation of NMDAR currents elicited by the two PAMs in the presence of either saturating (100 μM) or low (0.1 μM) pre-applied Glu. GNE-8324 potency was found to be strongly dependent on Glu concentration, while there was only a modest effect of Glu concentration on GNE-6901 potency (Figures 6G–6I, S6C, S6F, and S6G). Thus, while both GNE-6901 and GNE-8324 enhance the NMDAR current during Glu application, these two PAMs have striking differences. Compared to GNE-6901, GNE-8324 exhibits the following: (1) greater slowing of glutamate deactivation kinetics, (2) greater impact on NMDAR Glu potency, and (3) greater dependence of its potency on Glu concentration. These results suggest that, while both GNE-6901 and GNE-8324 are GluN2A-selective PAMs, their modes of action differ, potentially resulting in different effects during physiological activation of NMDARs.

Differential Impacts of GluN2A PAMs during Synaptic Plasticity Induction

To test the impacts of GNE-6901 and GNE-8324 in an intact circuit, we examined synaptic potentiation of Schaffer collateral inputs to CA1 pyramidal neurons. Short-term potentiation (STP) and long-term potentiation (LTP), two aspects of plasticity that depend on NMDAR activation (Malenka and Nicoll, 1993; Park et al., 2014), were assessed following one, two, and three bouts of a weak plasticity induction stimulus in the presence of vehicle (DMSO) or PAMs at concentrations expected to have near maximal effects (10 μM GNE-6901 and 30 μM GNE-8324). When potentiation was induced under physiological conditions, we observed an overall significant effect of treatment on LTP and STP (Figure 7A). Compared to vehicle, slices treated with GNE-6901 showed a trend toward enhanced LTP and exhibited significantly enhanced STP ($p < 0.001$), while slices treated with GNE-8324 showed a trend toward impaired LTP and exhibited significantly impaired STP ($p < 0.01$). Overall, both LTP ($p < 0.01$) and STP ($p < 0.001$) were significantly greater with GNE-6901 compared to GNE-8324 (Figure 7B).

NMDARs are present on both pyramidal neurons where they mediate induction of synaptic potentiation at the Schaffer collateral synapses, as well as on interneurons where they can contribute to polysynaptic inhibition of pyramidal neurons and oppose the induction of potentiation (Hanson et al., 2013). Therefore, the above results could potentially reflect a mixture of effects of GluN2A PAMs on pyramidal neurons and on interneurons recruited during plasticity induction. To examine the role of interneurons in the effects of the PAMs, we repeated these experiments in the presence of the $GABA_AR$ antagonist picrotoxin (PTX) to eliminate fast synaptic inhibition (Figures 7C and 7D). Under these conditions, GNE-6901 significantly potentiated both LTP ($p < 0.01$) and STP ($p < 0.001$). However, in contrast to the reduction of potentiation seen with GNE-8324 when inhibition was intact, in this experiment GNE-8324 had no effect on LTP and significantly enhanced STP ($p < 0.05$). Both LTP ($p < 0.01$) and STP ($p < 0.05$) were still significantly greater with GNE-6901 compared to GNE-8324 in the absence of inhibition. This impairment of synaptic potentiation by GNE-8324 in the presence, but not in the absence, of inhibition was confirmed in experiments using a stronger induction protocol (Figure S7).

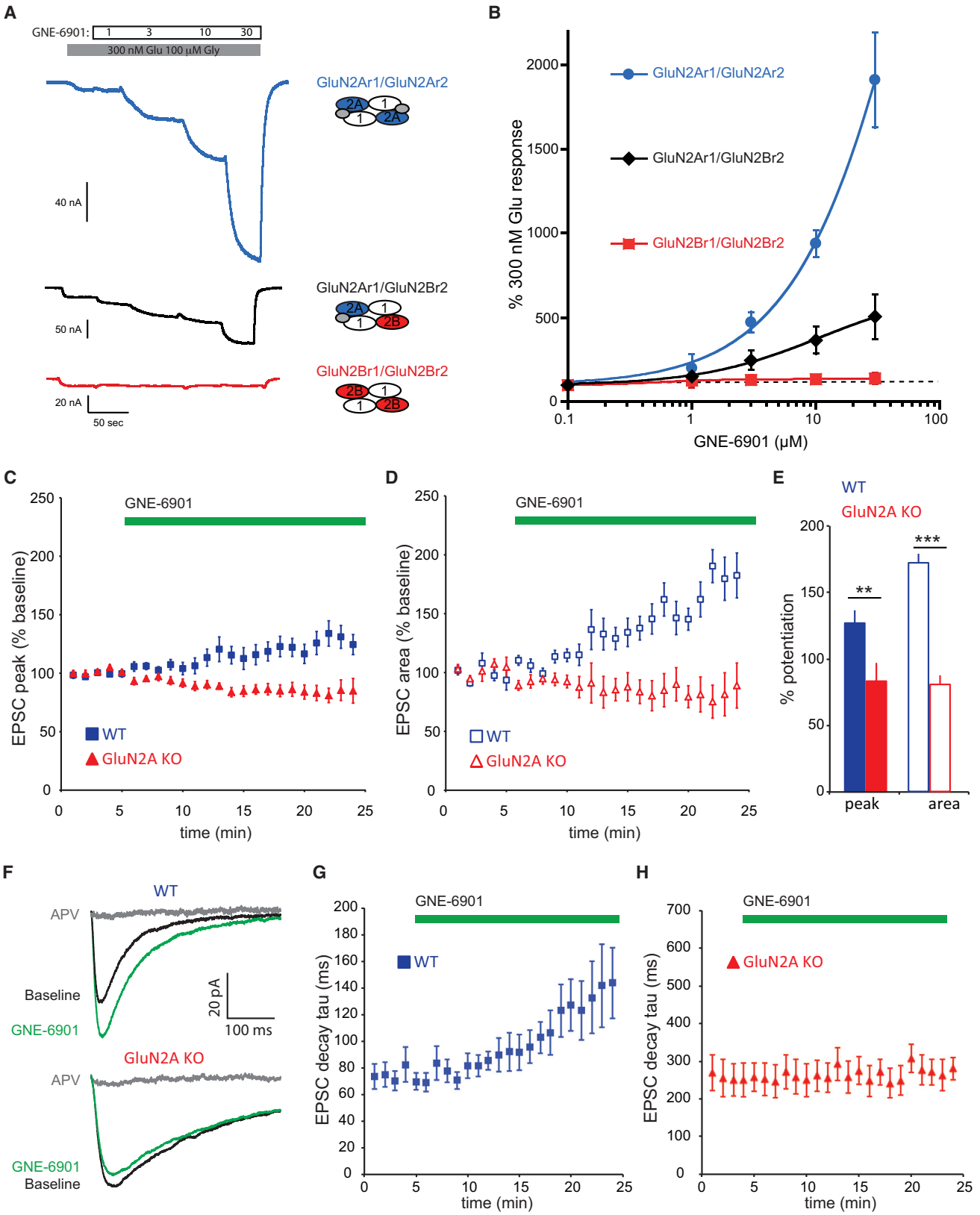

(legend on next page)

To better understand why GNE-8324 exhibits a relative lack of effect on plasticity with inhibition blocked but prominent effect with intact inhibition (while GNE-6901 enhances plasticity in both cases), we directly measured the impacts of each PAM on pyramidal neuron and interneuron NMDAR responses. While GNE-6901 significantly increased the area of synaptically activated NMDAR responses on pyramidal neurons ($p < 0.05$), GNE-8324 did not produce a significant effect (Figures 8A–8C). At the same time, whole-cell recordings targeting stratum radiatum interneurons showed that both PAMs significantly enhanced NMDAR EPSC area ($p < 0.01$) (Figures 8D–8F). Both PAMs delayed interneuron NMDAR EPSC decay to a similar magnitude as was observed with GNE-6901 in pyramidal neurons (Figure S8). The basis for the unequal ability of GNE-8324 to potentiate interneuron versus pyramidal neuron NMDARs could result from the unique biophysical properties of this PAM in combination with potential variations in synaptic neurotransmitter levels at different synapses.

To examine the PAM effects on NMDAR responses in the context of the bursts of stimulation that were used to induce LTP, isolated burst-evoked NMDARs were recorded from pyramidal neurons (Figure 8G). When inhibition was blocked, there was a small enhancement of burst-evoked responses by GNE-8324 that trended toward significance ($p = 0.14$), while GNE-6901 showed a more robust and significant enhancement ($p = 0.001$) (Figure 8H). This is consistent with the modest versus robust enhancement of NMDAR-dependent plasticity by GNE-8324 and GNE-6901, respectively. When these experiments were repeated with intact inhibition, GNE-8324 significantly impaired the burst-evoked NMDAR response ($p = 0.008$), while GNE-6901 continued to cause a significant enhancement ($p = 0.0005$) (Figure 8I), again paralleling the results of the NMDAR-dependent plasticity experiments. Overall these results suggest that, during plasticity induction, the robust pyramidal neuron impact of GNE-6901, but not GNE-8324, overrides the inhibition-dependent impacts of the PAMs. Thus, these two distinct GluN2A PAMs that differ in their impacts on NMDAR biophysical properties also differ in their effects during neuronal circuit function.

DISCUSSION

Here we report a novel class of NMDAR PAM that is selective for GluN2A subunit-containing NMDARs. Positive modulation and selectivity were demonstrated using multiple assay platforms on recombinant and native receptors including Ca^{2+} influx from cell lines and electrophysiology recordings from cell lines, *Xenopus* oocytes, and mouse brain slices. Importantly, triheteromeric GluN1/GluN2A/GluN2B receptors, which represent a major species of synaptic NMDARs, also could be potentiated, and enhancement of synaptically activated NMDARs in WT, but not GluN2A KO, mice confirmed the physiological selectivity of positive modulation established by the in vitro analyses.

The binding site of GluN2A PAMs at the GluN1-GluN2A heterodimer interface was identified using X-ray crystallography, which to our knowledge represents the first structure of an NMDAR modulator bound to the LBD region and, thus, defines a new site for allosteric modulation of NMDARs. Previous structural and functional analysis identified a critical role for the GluN1/GluN2 LBD dimer interface in NMDAR activation, leading to a model in which the aromatic side chain of GluN1 Y535 binds to a hydrophobic pocket in GluN2A, thus stabilizing the activated Glu-bound conformation (Furukawa et al., 2005). Interestingly, our structure shows that rotation of the GluN1 Y535 side chain is required to accommodate PAM binding, with the phenyl group of the PAM compounds instead mimicking the Y535 aromatic side chain (Figures 2C and 2D). While rotation of GluN1 Y535 out of this pocket is necessary to accommodate PAM binding, mutational analysis suggests the presence of this side chain is not essential for potentiation (Figure S2G). Overall we hypothesize that GluN2A PAMs stabilize the inter-domain interface to a greater extent than is achieved by the normal inter-subunit interactions that are displaced by PAM binding. This enhanced interaction between subunits is predicted to stabilize the Glu/Gly-bound conformation of the LBD and promote channel activation. Regarding selectivity, residue V783, which we demonstrated is critical for the GluN2A selectivity of our PAMs (Figure 2), previously was found to be important for the selective negative modulation of NMDARs by TCN-201 (Hansen et al., 2012). Notably, our crystal structure of a related NAM from the same class of compounds as TCN-201 shows a partially overlapping binding pocket with GluN2A PAMs, and we confirmed both unique and overlapping structural determinants for the classes of compounds (Figure 2). The convergence of the binding sites of two distinct classes of GluN2A-selective modulators with opposite effects on channel activity within an overlapping

Figure 4. Potentiation of Recombinant Triheteromeric NMDARs and Synaptically Activated NMDARs in Brain Slices

(A) Example GNE-6901 dose-response recordings from oocytes expressing GluN1 paired with GluN2Ar1/GluN2Ar2 (GluN2A diheteromers), GluN2Ar1/GluN2Br2 (GluN2A/GluN2B triheteromers), or GluN2Br1/GluN2Br2 (GluN2B diheteromers) are shown.

(B) GNE-6901 dose-response data for GluN2Ar1/GluN2Ar2, GluN2Ar1/GluN2Br2, or GluN2Br1/GluN2Br2 NMDARs. Cartoon representations of the NMDAR LBD subunit composition illustrate the 2, 1, and 0 PAM-binding sites (gray circles) in GluN2A diheteromers, GluN2A/GluN2B triheteromers, and GluN2B diheteromers, respectively. Data are shown as mean ± SD (n = 5–13 oocytes/dose).

(C and D) Isolated NMDAR EPSCs were recorded from WT or GluN2A KO mice. Baseline-normalized EPSC peak (A) and area (B) are shown during application of 30 μM GNE-6901. Data are shown as mean ± SEM (n = 10 WT mice and n = 6 KO mice). The gradual time course of compound effect may reflect penetration into the slice or use dependence.

(E) Potentiation of NMDAR EPSC peak and area in WT and GluN2A KO mice was calculated from the normalized current magnitude at the end of the recordings. Data are shown as mean ± SEM. WT potentiation of peak and area were significantly different from the GluN2A KO control (**$p < 0.01$ and ***$p < 0.001$).

(F) Example NMDAR EPSCs are shown during baseline (black), after 30 μM GNE-6901 application (green), and after blockade by 50 μM D-APV at the end of the experiment (gray). Note the slower time course of NMDAR EPSCs in GluN2A KO mice (scale bar represents 100 ms and 20 pA for both sets of traces).

(G and H) NMDAR EPSC decay time constants from single exponential fits of the falling portion of the EPSC are shown for slices from WT (E) and Glun2A KO mice (F) during GNE-6901 application.

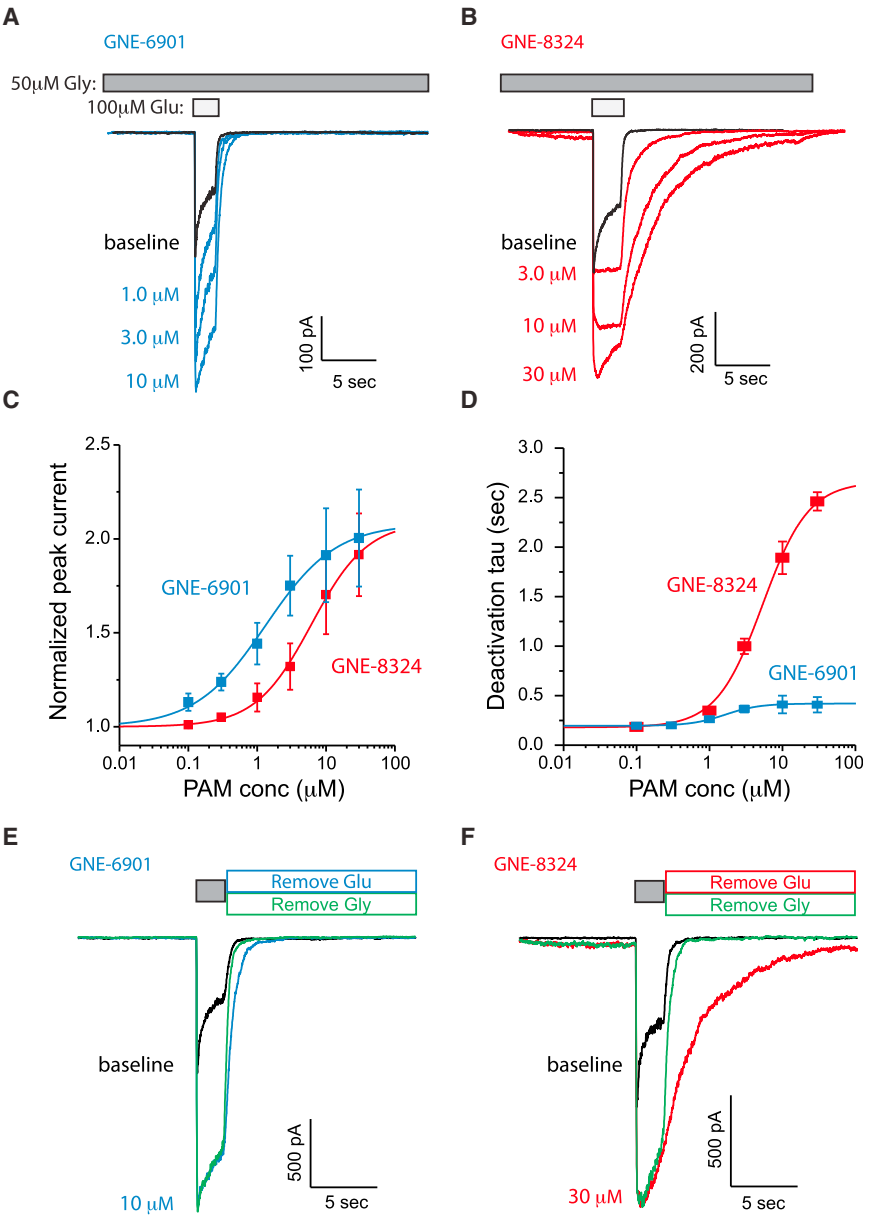

Figure 5. Effects of GNE-6901 and GNE-8324 on NMDAR Currents Using Rapid Agonist Application

(A) The dose dependence of GluN2A current potentiation is shown with overlaid traces of the NMDAR current in response to a brief application of 100 μM Glu in the constant presence of 50 μM Gly. Example traces are shown for baseline (black) and various concentrations of GNE-6901 (blue).

(B) The dose dependence of GluN2A current potentiation is shown for GNE-8324. Example traces are shown for baseline (black) and various concentrations of GNE-6901 (red). Note that while both GNE-6901 and GNE-8324 potentiate peak currents, only GNE-8324 significantly slows deactivation following the removal of Glu.

(C) GNE-6901 potentiates peak currents with an EC_{50} of 1.33 ± 0.22 μM and a maximum potentiation of 2.08 ± 0.42-fold over baseline, while GNE-8324 potentiates peak currents with an EC_{50} of 6.1 ± 1.06 μM and a maximum potentiation of 2.09 ± 0.27-fold over baseline. Data are shown as mean ± SEM (n = 5–7 patches/experiment).

(D) Deactivation kinetics are shown as a function of PAM concentration. GNE-6901 slows deactivation tau by 2.1 ± 0.71-fold over baseline (baseline tau = 186.2 ± 17.4 ms) with an EC_{50} of 1.64 ± 0.33 μM, while GNE-8324 slows tau by 14.8 ± 2.7-fold over baseline with an EC_{50} of 5.4 ± 1.6 μM. Note that GNE-8324 shows much greater slowing of deactivation kinetics relative to GNE-6901. Data are shown as mean ± SEM (n = 9–11 patches/experiment).

(E) Example recordings showing GluN2A currents either in the absence (baseline) or presence of 10 μM GNE-6901. The gray box represents the presence of both 100 μM Glu and 50 μM Gly. The black trace represents the baseline recording without GNE-6901 where Glu was removed in the presence of Gly, and the blue trace represents currents measured in the presence of 10 μM GNE-6901 where Glu was removed in the presence of Gly. The green trace represents the converse experiment where Gly was rapidly removed in the presence of Glu in the presence of 10 μM GNE-6901.

(F) Example recordings showing the same experimental paradigm as in (E) except with 30 μM GNE-8324. Note that delayed deactivation was only observed when Glu was removed in the presence of Gly, but not in the converse experiment.

inter-subunit interface underscores the unique value of this site for selective modulation of NMDARs.

The LBD plays a critical role in AMPAR and NMDAR activation (Mayer, 2011; Furukawa et al., 2005; Gielen et al., 2008) and is the binding site of AMPAR PAMs (Jin et al., 2005; Sun et al., 2002). While some of the identified NMDAR PAMs were found to achieve significant selectivity against AMPARs (Figure 3), the structural basis for this selectivity is not immediately obvious. Intriguingly, functional experiments showed that while the selective compound GNE-6901 had no significant effect on AMPARs by itself, it could compete with the AMPAR potentiation caused by GNE-3419 (Figure S3). One hypothesis to explain this interaction is that some of our compounds can function as SAMs at the LBD interface site of AMPARs, and, despite having no direct effect, can compete with the binding of compounds that do exhibit AMPAR PAM activity. We were not able to obtain a crystal structure of our AMPAR-selective compounds to verify this hypothesis. However, silent competitive inhibition of small-molecule modulators via inefficacious binding is not unprecedented, as exemplified by fluoxetine at the $GABA_AR$ benzodiazepine site (Rudolph and Knoflach, 2011) and substituted 4MP-TQS series compounds at nAChRs (Gill-Thind et al., 2015).

The detailed characterization of PAM effects on NMDAR channel function provides further insight into the basis of this allosteric modulation. In particular, the slowing of channel deactivation following removal of Glu, but not Gly (Figure 5), shows

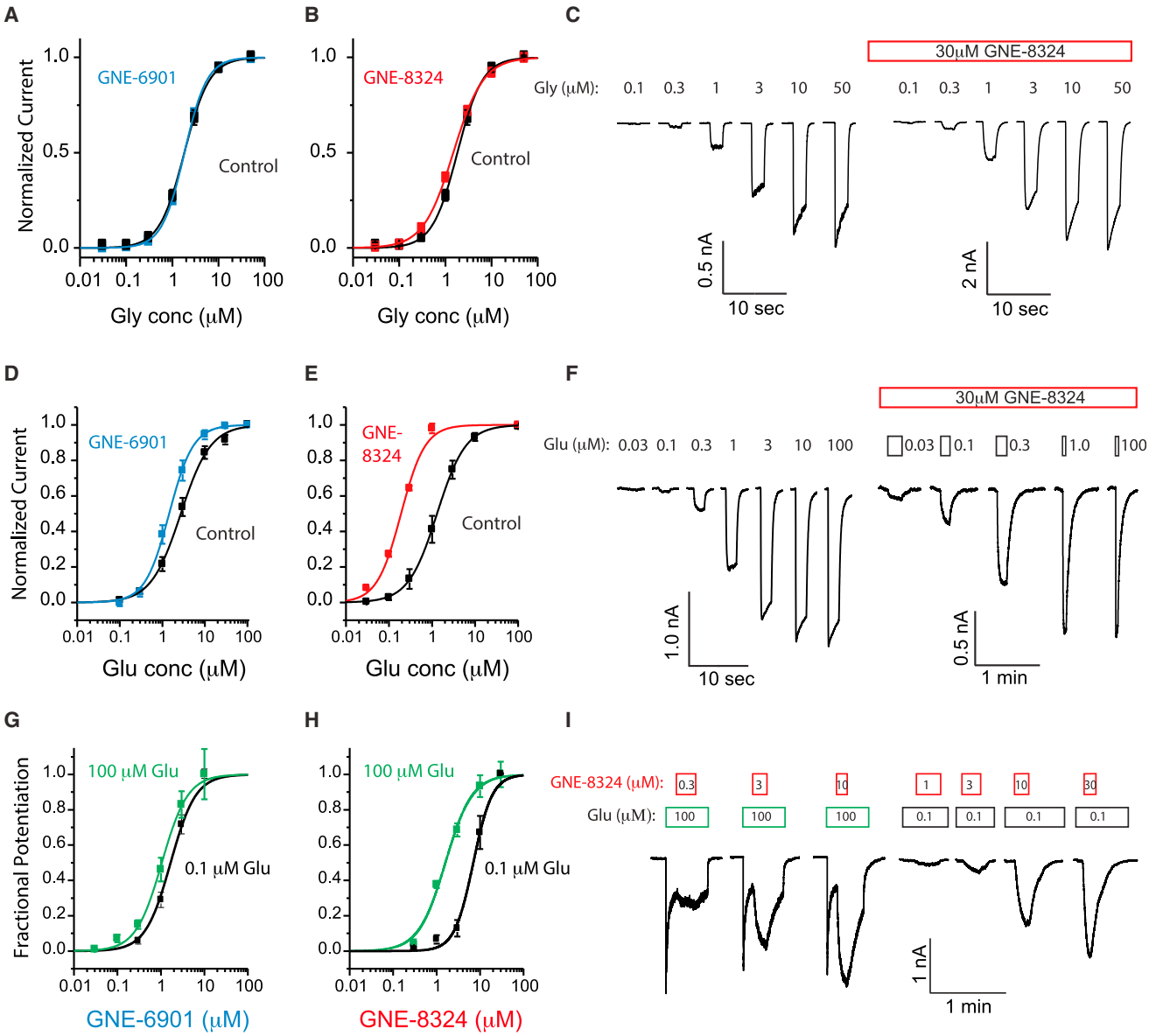

Figure 6. GNE-6901 and GNE-8324 Have Differential Effects on NMDAR Glu Potency and Differential Dependence on Glu Concentration

(A) Lack of effect of GNE-6901 (10 μM) on Gly potency (baseline EC_{50} = 1.82 ± 0.14 μM; GNE-6901 = 1.83 ± 0.16 μM; $p > 0.05$). Data are shown as mean ± SEM (n = 5–7 patches/experiment).

(B) Lack of effect of GNE-8324 (30 μM) on Gly potency (baseline EC_{50} = 1.82 ± 0.14 μM; GNE-8324 = 1.48 ± 0.2 μM; $p > 0.05$) is shown.

(C) GNE-8324 example traces. The EC_{50} for Gly was measured before and after the addition of 30 μM GNE-8324 in the continuous presence of 100 μM Glu. Brief 2-s pulses of Gly at varying concentrations were used to determine the EC_{50} values.

(D) Small effect of GNE-6901 (10 μM) on Glu potency (baseline EC_{50} = 2.7 ± 0.26 μM; GNE-6901 = 1.4 ± 0.35 μM; $p < 0.05$) is shown.

(E) Large effect of GNE-8324 (30 μM) on Glu potency (baseline EC_{50} = 1.3 ± 0.13 μM; GNE-8324 = 0.19 ± 0.05 μM; $p < 0.01$) is shown.

(F) GNE-8324 example traces. The EC_{50} for Glu was measured before and after the addition of 30 μM GNE-8324 in the continuous presence of 50 μM Gly. Brief 2-s pulses of Glu at various concentrations were used to determine the EC_{50} values.

(G) Small effect of Glu concentration on GNE-6901 EC_{50} (low Glu EC_{50} = 1.7 ± 0.12 μM; high Glu = 1.0 ± 0.27 μM; $p < 0.05$) is shown.

(H) Large effect of Glu on GNE-8324 EC_{50} (low Glu EC_{50} = 7.1 ± 1.3 μM; high Glu = 1.59 ± 0.12 μM; $p < 0.01$) is shown.

(I) GNE-8324 example traces. Pulses of GNE-8324 at various concentrations were tested in the presence of either low Glu (0.1 μM) or high Glu (100 μM), all in the continuous presence of 50 μM Gly. Examples of continuously recorded raw data for all experiments in this figure with GNE-6901 and GNE-8324 are shown in Figure S6.

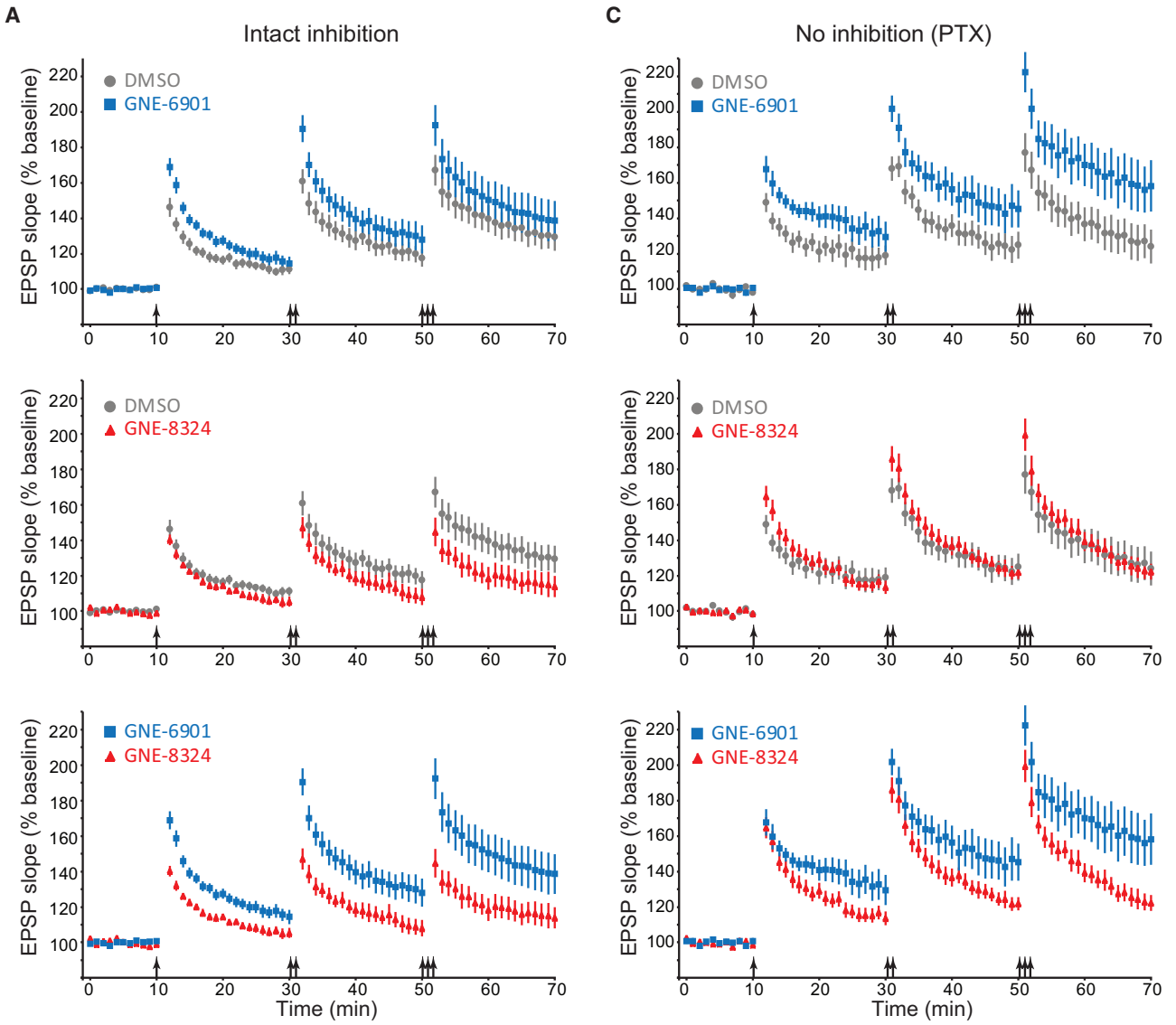

(legend on next page)

that while the modulator-binding site is located between the binding sites for the agonist and co-agonist, only Glu deactivation kinetics is affected. This is supported by the shift in NMDAR Glu, but not Gly, potency in the presence of GluN2A PAMs (Figure 6). Thus, while both GNE-6901 and GNE-8324 enhanced NMDAR currents during saturating agonist application, these compounds were differentiated by the magnitude of effects on Glu potency and slowing of deactivation following Glu removal, with GNE-8324 having much larger effects. A simple model of the transitions between unbound LBDs, LBDs bound by either PAM or Glu, and LBDs bound by both PAM and Glu, predicts that the magnitude of PAM effect on Glu affinity should be roughly equivalent to the magnitude of Glu effect on PAM affinity (Figures S6H–S6J). Indeed, this is what we observed, with a small impact of GNE-6901 on Glu potency (<2-fold shift), matching the small dependence of GNE-6901 potency on Glu concentration (<2-fold shift), and a larger impact of GNE-8324 on Glu potency (6.8-fold shift), approximately matching the larger dependence of GNE-8324 potency on Glu concentration (4.5-fold shift) (Figure 6). The structural basis for the differences in the nature of potentiation by GNE-6901 and GNE-8324 is not obvious from our data, however, as alignment of the crystal structures of compound-bound LBDs only show subtle differences.

In addition to qualitative differences at the level of NMDAR current modulation, GNE-6901 and GNE-8324 also showed qualitative differences in their impacts during LTP induction (Figure 7). Under basal recording conditions, these compounds exerted opposite effects on synaptic plasticity, with GNE-6901 significantly enhancing and GNE-8324 significantly impairing STP, and similar opposite trends were observed for the impacts of the PAMs on LTP. However, when inhibition, which can be recruited by polysynaptic activation during plasticity induction, was blocked, GNE-8324 no longer impaired plasticity, but rather a small but significant enhancement of STP was seen. At the same time, an even more robust enhancement of plasticity by GNE-6901 was seen in the absence of inhibition. These results suggest that, in general, GluN2A PAMs can have at least two sites of action during plasticity induction as follows: (1) potentiation of pyramidal neuron NMDARs, which directly mediate STP and LTP (Malenka and Nicoll, 1993; Park et al., 2014); and (2) potentiation of NMDARs on interneurons, which results in interneuron activation and pyramidal neuron hyperpolarization, thus opposing induction of synaptic potentiation.

Direct measurement of NMDAR responses in pyramidal neurons and interneurons showed that, while both PAMs enhance interneuron NMDARs, GNE-6901, but not GNE-8324, enhances pyramidal neuron NMDARs (Figure 8). Thus, the differential plasticity impacts can be explained by the dominance of pyramidal neuron effects of GNE-6901 over inhibition-dependent effects, while in the case of GNE-8324, inhibition-dependent effects dominate due to the lack of pyramidal neuron effects. One possibility is that the relative lack of GNE-8324 effects on pyramidal neurons derives from the significantly greater glutamate dependence of GNE-8324 compared to GNE-6901 (Figures 6G and 6H). This could hamper the ability of GNE-8324 to impact NMDARs at synapses onto pyramidal neurons where high-density transporters on astrocytes rapidly clear extracellular glutamate to maintain very low synaptic glutamate levels within milliseconds of presynaptic release (Clements et al., 1992). On the other hand, we speculate that astrocyte membranes near hippocampal interneurons could contain lower transporter densities than those surrounding synapses on pyramidal neurons, thus allowing stronger effects of Glu-dependent PAMs. This would be similar to the case in the cerebellum, where parallel fiber synapses onto interneurons are surrounded by lower transporter densities than those synapsing onto Purkinje cells (Chaudhry et al., 1995).

Overall, the identification of compounds that allow selective positive modulation of GluN2A NMDARs should be useful for dissecting NMDAR activation mechanisms, exploring cell-type-specific roles for GluN2A-containing NMDARs, and understanding the roles of GluN2A NMDARs in various brain circuits. These tools will not only provide insight into the physiological roles of GluN2A-containing NMDARs but also offer a means to test potential therapeutic benefits of NMDAR enhancement in model systems related to schizophrenia, epilepsy, and Alzheimer's and other diseases. For example, while current efforts to target NMDAR hypofunction in schizophrenia have relied on indirect and nonspecific enhancement of NMDARs via elevating Gly levels or activating mGluRs (Dunlop and Brandon, 2015), we have demonstrated that direct and selective pharmacological enhancement of GluN2A-containing NMDARs is possible.

Figure 7. Differential Effects of GNE-6901 and GNE-8324 on LTP Induction

(A) LTP was induced with one, then two, then three bouts of a weak induction protocol (arrows). Experiments were performed in the presence of 10 μM GNE-6901 (blue, n = 13 slices), 30 μM GNE-8324 (red, n = 12 slices), or DMSO vehicle control (gray, n = 12). For clarity, data from each pair of conditions are plotted separately (shown as mean ± SEM). PAM concentrations were selected based on having approximate maximal effects on peak current recorded from GluN2A cell lines.

(B) LTP was quantified as the average baseline-normalized EPSP slope during the last 5 min of each portion of the experiment (following one, two, or three bouts). There was a significant effect of treatment ($F(2,101) = 6.24$; $p = 0.003$) and bout number ($F(2,101) = 5.52$; $p = 0.005$) on LTP, but no significant interaction between treatment and bout number ($F(4,101) = 0.34$; $p = 0.85$). STP was quantified from the normalized EPSP slope of the data point collected 1 min after induction. There was a significant effect of treatment ($F(2,101) = 23.30$; $p < 0.001$) and bout number ($F(2,101) = 4.39$; $p = 0.015$) on STP, but no significant interaction between treatment and bout number ($F(4,101) = 0.55$; $p = 0.70$). Data are shown as mean ± SEM. Additional statistical analysis of comparisons between treatment groups is reported in the main text.

(C) LTP experiments were performed as in (A) but in the presence of 100 μM PTX to block synaptic inhibition (GNE-6901, n = 11; GNE-8324, n = 11; DMSO, n = 12).

(D) LTP and STP in the presence of PTX were quantified as in (B). There was a significant effect of treatment ($F(2,93) = 8.00$; $p < 0.001$), but not bout number ($F(2,93) = 2.51$; $p = 0.087$) on LTP. There was a significant effect of treatment ($F(2,93) = 12.13$; $p < 0.001$) and bout ($F(2,93) = 17.51$; $p < 0.001$) on STP, but no significant interaction between treatment and bout number ($F(4,93) = 0.71$; $p = 0.59$). Data are shown as mean ± SEM and additional statistical analysis of comparisons between treatment groups is reported in the main text.

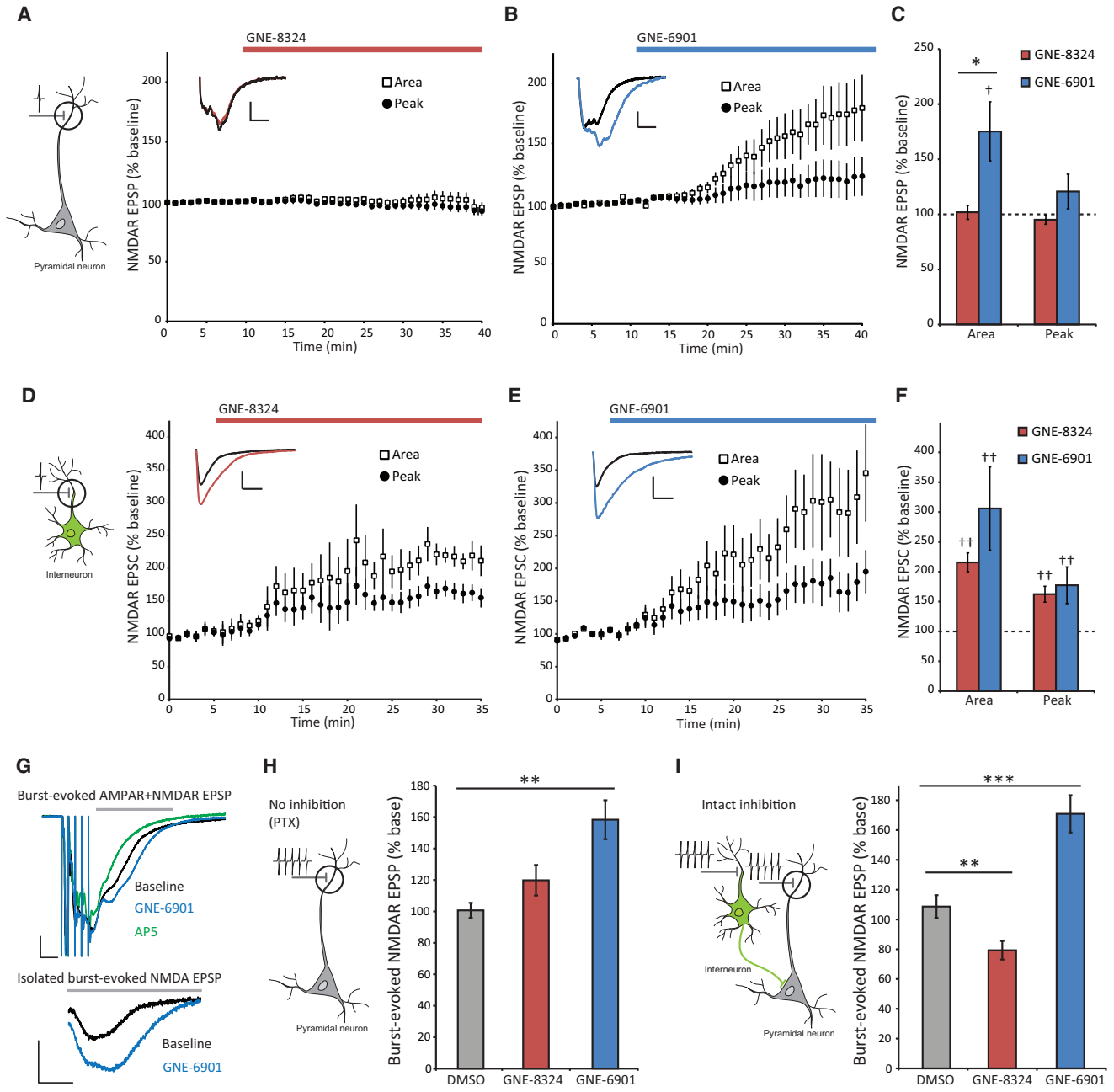

Figure 8. Effects of GNE-6901 and GNE-8324 on Pyramidal Neuron and Interneuron NMDAR Responses

(A) Isolated NMDAR EPSPs were recorded from CA1 pyramidal neurons in response to single electrical stimulations of presynaptic fibers. Application of 30 μM GNE-8324 had little effect on pyramidal neuron NMDAR EPSPs (n = 9, example traces are inset; scale bars, 0.25 mV and 50 ms).

(B) Application of 10 μM GNE-6901 potentiated pyramidal neuron NMDAR EPSPs (n = 10, example traces are inset; scale bars, 0.25 mV and 50 ms).

(C) GNE-6901 significantly enhanced the pyramidal neuron NMDAR EPSP area measured at the last 5 min of the recording compared to baseline (†$p < 0.05$). The NMDAR EPSP area at the end of the experiment was significantly greater for GNE-6901 compared to GNE-8324 (*$p < 0.05$).

(D) Isolated NMDAR EPSCs were recorded using whole-cell recordings targeted to GFP-positive neurons in the stratum radiatum of CA1 from GAD67-GFP reporter mice. Application of 30 μM GNE-8324 potentiated interneuron NMDAR EPSCs (n = 9, example traces are inset; scale bars, 100 pA and 50 ms).

(E) Application of 10 μM GNE-6901 potentiated interneuron NMDAR EPSCs (n = 9, example traces are inset; scale bars, 100 pA and 50 ms).

(F) GNE-6901 and GNE-8324 both significantly enhanced the peak and area of interneuron NMDAR EPSCs measured at the last 5 min of the recording compared to baseline (††$p < 0.01$). Neither NMDAR EPSC area nor peak at the end of the experiment significantly differed between GNE-6901 and GNE-8324 ($p > 0.05$).

(G) Burst-evoked NMDAR EPSPs in pyramidal neurons were measured in response to five pulses at 100 Hz. Because burst-evoked responses were observed to run down under the conditions for isolated NMDAR EPSPs, mixed AMPAR + NMDAR EPSPs were measured, which allowed a stable baseline response to be obtained. After recordings stabilized, PAM was applied for 40 min, followed by D-AP5 application to block the NMDAR component of the response (top).

(legend continued on next page)

Although the compounds reported here do not have appropriate properties for use in vivo, the discovery of a new allosteric site at the LBD interface expands on the previous knowledge of NMDAR allosteric sites, which previously have been mostly restricted to the ATD region (Zhu and Paoletti, 2015). Similar to AMPARs, the LBD dimer interface now emerges as a key allosteric locus for fine-tuning of NMDAR activity in a subunit-specific manner, which should provide the basis for future development of therapeutics for brain disorders.

EXPERIMENTAL PROCEDURES

Additional details of the procedures are provided in the Supplemental Experimental Procedures.

Cell Lines

Doxycycline-inducible (Dox) cell lines that express either GluN1/GluN2A or GluN1/GluN2B were generated in both CHO and HEK293 parental cell lines, and Dox-inducible cell lines that express either GluN1/GluN2C or GluN1/GluN2D were obtained from Chantest. The cDNAs for Dox-inducible cell lines that express either the flip or flop isoform of the human GluA2 AMPAR included a Gln at position 607 to impart Ca^{2+} permeability (which is absent when there is an Arg at this position as normally results from highly efficient RNA editing of the Gln codon in genomic DNA) in order to enable Ca^{2+} influx assays.

Ca^{2+} Influx Assays

The HTS of 1.4 million compounds was conducted using a Ca^{2+} influx assay utilizing GluN1/GluN2A-expressing HEK cells. Cells were loaded with a Ca^{2+}-sensitive dye and plated in acidic buffer to prevent channel opening. The proton block was reversed at the time of assay by the addition of test compound in neutralizing buffer containing saturating glycine. Endogenous glutamate from cells was present at a concentration producing submaximal activation, allowing for detection of compounds that enhance NMDAR Ca^{2+} influx.

Purification and Crystallization of the GluN1/GluN2A and GluA2 LBD Complexes

For the human GluN1 LBD, a construct containing residues M394–K544 (S1) and R663–S800 (S2) connected by a Gly-Thr linker was generated based on the strategy for rat GluN1 LBD (Furukawa and Gouaux, 2003). The human GluN2A LBD construct, containing residues P401–R539 (S1) and Q661–N802 (S2) connected by a Gly-Thr linker, was based on the strategy for rat GluN2A LBD (Furukawa et al., 2005). For the human GluA2 LBD, a construct (previously described as S1S2J variant) was generated containing residues N392–K506 (S1) and P632–S775 (S2) connected by a Gly-Thr linker (Armstrong and Gouaux, 2000). This construct contained GluA2 flip residue Ser754 and flop residues Asn744, Ala745, and Leu758.

Animals

All animal studies were approved by the Genentech Institutional Animal Care and Use Committee (IACUC) and conducted in accordance with the NIH Guide for the Care and Use of Laboratory Animals. The 6- to 9-week-old GluN2A KO mice (Kadotani et al., 1996) and WT littermates were used for whole-cell recordings from pyramidal neurons, and GAD67-GFP knockin mice were used when targeting interneurons. The 2- to 3-month-old C57BL/6 mice were used for field recordings.

Electrophysiology

For two-electrode voltage-clamp (TEVC) recordings of diheteromeric NMDARs, *Xenopus* oocytes were injected with mRNA for hGluN1-1a and hGluN2A or hGluN2B, using either WT or mutant mRNA. Experiments comparing GluN1-1a and GluN1-1b splice variants were performed using rGluN1-1a, rGluN1-1b, and rGluN2A. Similarly, experiments with chimeric/deleted ATD subunits were performed using rodent clones. Selective expression of triheteromeric NMDARs in *Xenopus* oocytes was performed as previously described (Stroebel et al., 2014).

Whole-cell patch-clamp recordings from cell lines were performed using the Dynaflow Resolve rapid solution exchange system (Cellectricon). This system consists of a quartz glass perfusion chip with a linear array of 16 continuously flowing perfusion channels that are moved past the patched cell with a solution exchange time of ~10–30 ms.

Field EPSP recordings were made from the stratum radiatum of area CA1 of the hippocampus in response to electrical stimulation of the Schaffer collateral pathway. For experiments examining the direct effects of compounds on AMPAR EPSPs, 50 μM D-(-)-2-amino-5-phosphonopentanoic acid (AP5) was included. Field NMDAR EPSPs were recorded in the presence of 10 μM NBQX, 100 μM PTX, and 10 μM strychnine with reduced Mg^{2+} (0.2 mM). For plasticity experiments, a single bout of weak induction stimuli consisted of five pulses at 100 Hz, and plasticity was induced using one, two, or three bouts of this protocol (30-s inter-bout interval). EPSP measurement resumed 1 min after induction so that post-tetanic potentiation (PTP), which is a presynaptic phenomenon, did not contribute to the measurement of STP, which, along with LTP, is a postsynaptic NMDAR-dependent phenomenon (Malenka and Nicoll, 1993; Park et al., 2014). Statistical significances of LTP and STP were assessed using a two-way ANOVA with treatment and bout number as factors, and burst-evoked EPSPs were assessed with a one-way ANOVA with treatment as a factor. When there was a significant effect of treatment, follow-up tests assessing significance of differences between different treatments were performed using the Holm-Sidak method. In experiments where only two groups were compared, significance was assessed using a t test.

Whole-cell recordings of NMDAR EPSCs in CA1 pyramidal neurons in response to local stimulation were recorded at a holding potential of −70 mV in the presence of reduced Mg^{2+} (0.5 mM), and they were isolated using 10 μM NBQX disodium salt and 100 μM PTX. AP5 applied at the end of the recording confirmed isolation of pure NMDAR EPSCs.

ACCESSION NUMBERS

The accession numbers for the structures reported in this paper are PDB: 5H8F (apo GluN1/N2A), 5H8H (GNE3419 GluN1/N2A), 5H8N (compound 6 GluN1/N2A), 5H8Q (GNE8324 GluN1/N2A), 5H8R (GNE6901 GluN1/N2A), and 5H8S (GNE3419 GluA1).

SUPPLEMENTAL INFORMATION

Supplemental Information includes Supplemental Experimental Procedures, eight figures, and one table and can be found with this article online at http://dx.doi.org/10.1016/j.neuron.2016.01.016.

Subtraction of the isolated AMPA response measured in AP5 was used to calculate the baseline and PAM-treated NMDAR EPSPs (bottom). To minimize contamination from stimulus artifacts and population spikes, the burst-evoked NMDAR EPSP was quantified from the portion of the response immediately following stimulation (gray bar). Scale bars, 0.5 mV and 25 ms.

(H) When burst-evoked NMDAR EPSPs were recorded with inhibition blocked (n = 10, GNE-6901; n = 11, GNE-8324; n = 12, DMSO), there was a significant effect of treatment ($F(2,30) = 10.52$; $p < 0.001$), which corresponded with a trend toward increased area with GNE-8324 and a significant increase with GNE-6901 compared to vehicle (**$p < 0.01$).

(I) When burst-evoked NMDAR EPSPs were recorded with intact inhibition (n = 11, GNE-6901; n = 12, GNE-8324; n = 10, DMSO), there was a significant effect of treatment ($F(2,30) = 26.99$; $p < 0.001$), which corresponded with a significantly reduced area with GNE-8324 (**$p < 0.01$) and a significantly increased area with GNE-6901 compared to vehicle (**$p < 0.001$).

Data are shown as mean ± SEM.

AUTHOR CONTRIBUTIONS

D.H.H., P.J.L., P.P., M.S., Q.Z., and J.E.H. conceived and designed experiments. D.H.H., P.J.L., T.G., Y.C., T.-M.W., P.R., A.G., H.J.A.W., and J.E.H. conducted experiments. M.V., B.D.S., and J.B.S. designed and synthesized chemicals. D.H.H., P.J.L., P.P., M.S., and J.E.H. wrote the paper.

ACKNOWLEDGMENTS

The authors thank Kimberly Scearce-Levie and Justin Elstrott for providing valuable comments on the manuscript, Yichin Liu and James Herrington for advice on the design of Ca^{2+} influx assays, Antonio DiPasquale (UC Berkeley X-ray Crystallography Facility) for small molecule X-ray crystallography support, and Pharmaron for chemistry support. The Stanford Synchrotron Radiation Lightsource (SSRL) is supported by the U.S. Department of Energy (DOE) Office of Science under contract DE-AC02-76SF00515. The SSRL Structural Molecular Biology Program is supported by the DOE Office of Biological and Environmental Research and by the NIH, National Institute of General Medical Sciences (including P41GM103393). Beamline 08ID-1 at the Canadian Light Source is supported by the Natural Sciences and Engineering Research Council of Canada, the National Research Council Canada, the Canadian Institutes of Health Research, the Province of Saskatchewan, Western Economic Diversification Canada, and the University of Saskatchewan. The Advanced Photon Source is a U.S. DOE Office of Science User Facility operated by Argonne National Laboratory under contract DE-AC02-06CH11357. T.G. and P.P were supported by grants from the Pierre-Gilles-de-Gennes Foundation and the Fondation pour la Recherche Médicale (FRM, Equipe FRM DEQ20130326520). D.H.H., P.J.L., T.-M.W., P.R., A.G., H.J.A.W., M.V., B.D.S., J.B.S., M.S., Q.Z., and J.E.H. are current or former employees of Genentech, Inc.

Received: June 19, 2015
Revised: November 24, 2015
Accepted: January 6, 2016
Published: February 11, 2016

REFERENCES

Armstrong, N., and Gouaux, E. (2000). Mechanisms for activation and antagonism of an AMPA-sensitive glutamate receptor: crystal structures of the GluR2 ligand binding core. Neuron *28*, 165–181.

Belforte, J.E., Zsiros, V., Sklar, E.R., Jiang, Z., Yu, G., Li, Y., Quinlan, E.M., and Nakazawa, K. (2010). Postnatal NMDA receptor ablation in corticolimbic interneurons confers schizophrenia-like phenotypes. Nat. Neurosci. *13*, 76–83.

Bettini, E., Sava, A., Griffante, C., Carignani, C., Buson, A., Capelli, A.M., Negri, M., Andreetta, F., Senar-Sancho, S.A., Guiral, L., and Cardullo, F. (2010). Identification and characterization of novel NMDA receptor antagonists selective for NR2A- over NR2B-containing receptors. J. Pharmacol. Exp. Ther. *335*, 636–644.

Carvill, G.L., Regan, B.M., Yendle, S.C., O'Roak, B.J., Lozovaya, N., Bruneau, N., Burnashev, N., Khan, A., Cook, J., Geraghty, E., et al. (2013). GRIN2A mutations cause epilepsy-aphasia spectrum disorders. Nat. Genet. *45*, 1073–1076.

Chaudhry, F.A., Lehre, K.P., van Lookeren Campagne, M., Ottersen, O.P., Danbolt, N.C., and Storm-Mathisen, J. (1995). Glutamate transporters in glial plasma membranes: highly differentiated localizations revealed by quantitative ultrastructural immunocytochemistry. Neuron *15*, 711–720.

Clements, J.D., Lester, R.A., Tong, G., Jahr, C.E., and Westbrook, G.L. (1992). The time course of glutamate in the synaptic cleft. Science *258*, 1498–1501.

Costa, R.O., Lacor, P.N., Ferreira, I.L., Resende, R., Auberson, Y.P., Klein, W.L., Oliveira, C.R., Rego, A.C., and Pereira, C.M. (2012). Endoplasmic reticulum stress occurs downstream of GluN2B subunit of N-methyl-d-aspartate receptor in mature hippocampal cultures treated with amyloid-β oligomers. Aging Cell *11*, 823–833.

Coyle, J.T., Tsai, G., and Goff, D. (2003). Converging evidence of NMDA receptor hypofunction in the pathophysiology of schizophrenia. Ann. N Y Acad. Sci. *1003*, 318–327.

Dunlop, J., and Brandon, N.J. (2015). Schizophrenia drug discovery and development in an evolving era: are new drug targets fulfilling expectations? J. Psychopharmacol. (Oxford) *29*, 230–238.

Ferreira, I.L., Bajouco, L.M., Mota, S.I., Auberson, Y.P., Oliveira, C.R., and Rego, A.C. (2012). Amyloid beta peptide 1-42 disturbs intracellular calcium homeostasis through activation of GluN2B-containing N-methyl-d-aspartate receptors in cortical cultures. Cell Calcium *51*, 95–106.

Furukawa, H., and Gouaux, E. (2003). Mechanisms of activation, inhibition and specificity: crystal structures of the NMDA receptor NR1 ligand-binding core. EMBO J. *22*, 2873–2885.

Furukawa, H., Singh, S.K., Mancusso, R., and Gouaux, E. (2005). Subunit arrangement and function in NMDA receptors. Nature *438*, 185–192.

Gielen, M., Le Goff, A., Stroebel, D., Johnson, J.W., Neyton, J., and Paoletti, P. (2008). Structural rearrangements of NR1/NR2A NMDA receptors during allosteric inhibition. Neuron *57*, 80–93.

Gill-Thind, J.K., Dhankher, P., D'Oyley, J.M., Sheppard, T.D., and Millar, N.S. (2015). Structurally similar allosteric modulators of α7 nicotinic acetylcholine receptors exhibit five distinct pharmacological effects. J. Biol. Chem. *290*, 3552–3562.

Gonzalez-Burgos, G., and Lewis, D.A. (2012). NMDA receptor hypofunction, parvalbumin-positive neurons, and cortical gamma oscillations in schizophrenia. Schizophr. Bull. *38*, 950–957.

Gray, J.A., Shi, Y., Usui, H., During, M.J., Sakimura, K., and Nicoll, R.A. (2011). Distinct modes of AMPA receptor suppression at developing synapses by GluN2A and GluN2B: single-cell NMDA receptor subunit deletion in vivo. Neuron *71*, 1085–1101.

Hansen, K.B., Ogden, K.K., and Traynelis, S.F. (2012). Subunit-selective allosteric inhibition of glycine binding to NMDA receptors. J. Neurosci. *32*, 6197–6208.

Hansen, K.B., Ogden, K.K., Yuan, H., and Traynelis, S.F. (2014). Distinct functional and pharmacological properties of Triheteromeric GluN1/GluN2A/GluN2B NMDA receptors. Neuron *81*, 1084–1096.

Hanson, J.E., Weber, M., Meilandt, W.J., Wu, T., Luu, T., Deng, L., Shamloo, M., Sheng, M., Scearce-Levie, K., and Zhou, Q. (2013). GluN2B antagonism affects interneurons and leads to immediate and persistent changes in synaptic plasticity, oscillations, and behavior. Neuropsychopharmacology *38*, 1221–1233.

Hardingham, G.E., and Bading, H. (2010). Synaptic versus extrasynaptic NMDA receptor signalling: implications for neurodegenerative disorders. Nat. Rev. Neurosci. *11*, 682–696.

Hatton, C.J., and Paoletti, P. (2005). Modulation of triheteromeric NMDA receptors by N-terminal domain ligands. Neuron *46*, 261–274.

Heng, M.Y., Detloff, P.J., Wang, P.L., Tsien, J.Z., and Albin, R.L. (2009). In vivo evidence for NMDA receptor-mediated excitotoxicity in a murine genetic model of Huntington disease. J. Neurosci. *29*, 3200–3205.

Javitt, D.C., and Zukin, S.R. (1991). Recent advances in the phencyclidine model of schizophrenia. Am. J. Psychiatry *148*, 1301–1308.

Jin, R., Clark, S., Weeks, A.M., Dudman, J.T., Gouaux, E., and Partin, K.M. (2005). Mechanism of positive allosteric modulators acting on AMPA receptors. J. Neurosci. *25*, 9027–9036.

Kadotani, H., Hirano, T., Masugi, M., Nakamura, K., Nakao, K., Katsuki, M., and Nakanishi, S. (1996). Motor discoordination results from combined gene disruption of the NMDA receptor NR2A and NR2C subunits, but not from single disruption of the NR2A or NR2C subunit. J. Neurosci. *16*, 7859–7867.

Karakas, E., and Furukawa, H. (2014). Crystal structure of a heterotetrameric NMDA receptor ion channel. Science *344*, 992–997.

Krystal, J.H., Karper, L.P., Seibyl, J.P., Freeman, G.K., Delaney, R., Bremner, J.D., Heninger, G.R., Bowers, M.B., Jr., and Charney, D.S. (1994). Subanesthetic effects of the noncompetitive NMDA antagonist, ketamine, in

humans. Psychotomimetic, perceptual, cognitive, and neuroendocrine responses. Arch. Gen. Psychiatry *51*, 199–214.

Lee, C.H., Lü, W., Michel, J.C., Goehring, A., Du, J., Song, X., and Gouaux, E. (2014). NMDA receptor structures reveal subunit arrangement and pore architecture. Nature *511*, 191–197.

Lemke, J.R., Lal, D., Reinthaler, E.M., Steiner, I., Nothnagel, M., Alber, M., Geider, K., Laube, B., Schwake, M., Finsterwalder, K., et al. (2013). Mutations in GRIN2A cause idiopathic focal epilepsy with rolandic spikes. Nat. Genet. *45*, 1067–1072.

Lesca, G., Rudolf, G., Bruneau, N., Lozovaya, N., Labalme, A., Boutry-Kryza, N., Salmi, M., Tsintsadze, T., Addis, L., Motte, J., et al. (2013). GRIN2A mutations in acquired epileptic aphasia and related childhood focal epilepsies and encephalopathies with speech and language dysfunction. Nat. Genet. *45*, 1061–1066.

Liu, Y., Wong, T.P., Aarts, M., Rooyakkers, A., Liu, L., Lai, T.W., Wu, D.C., Lu, J., Tymianski, M., Craig, A.M., and Wang, Y.T. (2007). NMDA receptor subunits have differential roles in mediating excitotoxic neuronal death both in vitro and in vivo. J. Neurosci. *27*, 2846–2857.

Malenka, R.C., and Nicoll, R.A. (1993). NMDA-receptor-dependent synaptic plasticity: multiple forms and mechanisms. Trends Neurosci. *16*, 521–527.

Martel, M.A., Ryan, T.J., Bell, K.F., Fowler, J.H., McMahon, A., Al-Mubarak, B., Komiyama, N.H., Horsburgh, K., Kind, P.C., Grant, S.G., et al. (2012). The subtype of GluN2 C-terminal domain determines the response to excitotoxic insults. Neuron *74*, 543–556.

Mayer, M.L. (2011). Emerging models of glutamate receptor ion channel structure and function. Structure *19*, 1370–1380.

Milnerwood, A.J., Gladding, C.M., Pouladi, M.A., Kaufman, A.M., Hines, R.M., Boyd, J.D., Ko, R.W., Vasuta, O.C., Graham, R.K., Hayden, M.R., et al. (2010). Early increase in extrasynaptic NMDA receptor signaling and expression contributes to phenotype onset in Huntington's disease mice. Neuron *65*, 178–190.

Mohn, A.R., Gainetdinov, R.R., Caron, M.G., and Koller, B.H. (1999). Mice with reduced NMDA receptor expression display behaviors related to schizophrenia. Cell *98*, 427–436.

Paoletti, P., Bellone, C., and Zhou, Q. (2013). NMDA receptor subunit diversity: impact on receptor properties, synaptic plasticity and disease. Nat. Rev. Neurosci. *14*, 383–400.

Park, P., Volianskis, A., Sanderson, T.M., Bortolotto, Z.A., Jane, D.E., Zhuo, M., Kaang, B.K., and Collingridge, G.L. (2014). NMDA receptor-dependent long-term potentiation comprises a family of temporally overlapping forms of synaptic plasticity that are induced by different patterns of stimulation. Philos. Trans. R. Soc. Lond. B Biol. Sci. *369*, 20130131.

Rauner, C., and Köhr, G. (2011). Triheteromeric NR1/NR2A/NR2B receptors constitute the major N-methyl-D-aspartate receptor population in adult hippocampal synapses. J. Biol. Chem. *286*, 7558–7566.

Rönicke, R., Mikhaylova, M., Rönicke, S., Meinhardt, J., Schröder, U.H., Fändrich, M., Reiser, G., Kreutz, M.R., and Reymann, K.G. (2011). Early neuronal dysfunction by amyloid β oligomers depends on activation of NR2B-containing NMDA receptors. Neurobiol. Aging *32*, 2219–2228.

Rudolph, U., and Knoflach, F. (2011). Beyond classical benzodiazepines: novel therapeutic potential of GABAA receptor subtypes. Nat. Rev. Drug Discov. *10*, 685–697.

Rujescu, D., Bender, A., Keck, M., Hartmann, A.M., Ohl, F., Raeder, H., Giegling, I., Genius, J., McCarley, R.W., Möller, H.J., and Grunze, H. (2006). A pharmacological model for psychosis based on N-methyl-D-aspartate receptor hypofunction: molecular, cellular, functional and behavioral abnormalities. Biol. Psychiatry *59*, 721–729.

Sheng, M., Cummings, J., Roldan, L.A., Jan, Y.N., and Jan, L.Y. (1994). Changing subunit composition of heteromeric NMDA receptors during development of rat cortex. Nature *368*, 144–147.

Soares, C., and Lee, K.F. (2013). A prominent role for triheteromeric GluN1/GluN2A/GluN2B NMDARs at central synapses. J. Neurosci. *33*, 14975–14977.

Soto, D., Altafaj, X., Sindreu, C., and Bayés, A. (2014). Glutamate receptor mutations in psychiatric and neurodevelopmental disorders. Commun. Integr. Biol. *7*, e27887.

Stroebel, D., Carvalho, S., Grand, T., Zhu, S., and Paoletti, P. (2014). Controlling NMDA receptor subunit composition using ectopic retention signals. J. Neurosci. *34*, 16630–16636.

Sun, Y., Olson, R., Horning, M., Armstrong, N., Mayer, M., and Gouaux, E. (2002). Mechanism of glutamate receptor desensitization. Nature *417*, 245–253.

Tovar, K.R., McGinley, M.J., and Westbrook, G.L. (2013). Triheteromeric NMDA receptors at hippocampal synapses. J. Neurosci. *33*, 9150–9160.

Traynelis, S.F., Wollmuth, L.P., McBain, C.J., Menniti, F.S., Vance, K.M., Ogden, K.K., Hansen, K.B., Yuan, H., Myers, S.J., and Dingledine, R. (2010). Glutamate receptor ion channels: structure, regulation, and function. Pharmacol. Rev. *62*, 405–496.

Tu, W., Xu, X., Peng, L., Zhong, X., Zhang, W., Soundarapandian, M.M., Balel, C., Wang, M., Jia, N., Zhang, W., et al. (2010). DAPK1 interaction with NMDA receptor NR2B subunits mediates brain damage in stroke. Cell *140*, 222–234.

Williams, K., Russell, S.L., Shen, Y.M., and Molinoff, P.B. (1993). Developmental switch in the expression of NMDA receptors occurs in vivo and in vitro. Neuron *10*, 267–278.

Zádori, D., Veres, G., Szalárdy, L., Klivényi, P., Toldi, J., and Vécsei, L. (2014). Glutamatergic dysfunctioning in Alzheimer's disease and related therapeutic targets. J. Alzheimers Dis. *42* (*Suppl 3*), S177–S187.

Zeron, M.M., Hansson, O., Chen, N., Wellington, C.L., Leavitt, B.R., Brundin, P., Hayden, M.R., and Raymond, L.A. (2002). Increased sensitivity to N-methyl-D-aspartate receptor-mediated excitotoxicity in a mouse model of Huntington's disease. Neuron *33*, 849–860.

Zhou, Q., and Sheng, M. (2013). NMDA receptors in nervous system diseases. Neuropharmacology *74*, 69–75.

Zhu, S., and Paoletti, P. (2015). Allosteric modulators of NMDA receptors: multiple sites and mechanisms. Curr. Opin. Pharmacol. *20*, 14–23.